ISSN:1575-6807
D.L.: GC-1317-1999

INSTITUTO UNIVERSITARIO DE CIENCIAS Y TECNOLOGIAS CIBERNETICAS

Optic Flow Estimation in Fluid Images II

L. Alvarez, C. Castaño, M.García, L. Mazorra, A. Salgado and J. Sánchez

Nº 0032

November 2005

Cuadernos del Instituto Universitario de Ciencias y Tecnologías Cibernéticas
Instituto Universitario de Ciencias y Tecnologías Cibernéticas
Universidad de Las Palmas de Gran Canaria
Campus de Tafira
35017 Las Palmas, España
http://www.iuctc.ulpgc.es

Optic flow estimation in fluid images II

L. Alvarez, C.A. Castaño, M. García, L. Mazorra, A. Salgado and J. Sánchez
Departamento de Informática y Sistemas.
Universidad de Las Palmas de Gran Canaria.
Campus de Tafira s/n. 35017 Las Palmas de Gran Canaria. SPAIN

November 20, 2005

Abstract

In this report we study a number of fluid optic flow sequences in the context of the FLUID Specific Targeted Research Project - Contract No 513633 founded by the EEC. The main goal of this report is to analyse the behaviour of classical computer vision optic flow techniques when we deal with fluid sequences. We use the optic flow sequences provided by other partners of the FLUID project.

1 Introduction

Fluid flow sequences are of a very special nature. We are going to study 2 types of fluid sequences. On the one hand, satellite sequences where we try to follow cloud structures. Here, the main problem is that the shape of cloud structures change a lot between 2 consecutive satellite images mainly because of 3D phenomena. On the other hand we are going to study PIV sequence characterized by a flow of particles that it is captured by CCD cameras. In order to have an idea about the behaviour of classical computer vision approach to the flow estimation in this kind of sequences we are going to perform a number of experiments using the optic flow sequences provided by other partners of the FLUID project.

In that sense, section 2 details the most important issues that should be addressed in order to unify a common framework to study the behaviour of different optic flow estimation methods. Then, section 3 shows a statistical analysis of the four methods we analyse in this report: Simple Flow (a PDE based approach), Video Flow (also a PDE based approach), a correlation based scheme and a structure tensor based approach. This report has not comparison purposes, we want just to explore the behaviour of standard computer vision methods in fluid sequences. In the future, and based on the results obtained here, we will propose new methods trying to overcome the main limitations we have found in the methods analysed here.

2 Methodology

The aim of the proposed methodology is to fit ideas in order to define a common framework for evaluating different optic flow estimation methods in the context of some fluid image sequences. To achieve this task, we propose the processing scheme represented on Fig. 1, where different image sequences can be used as input for the estimation method under analysis. Then, any optic flow estimation method, which is seen as a black box, is applied to calculate the motion through the image sequence which is stored as an ASCII file using the standard format detailed in section 2.3.

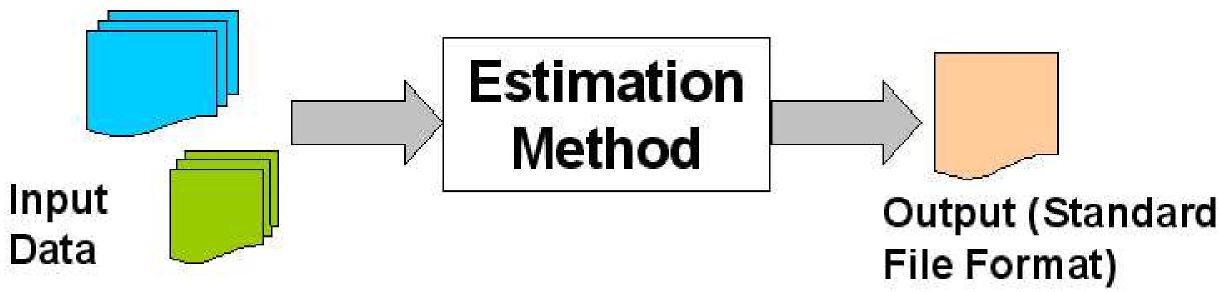

Figure 1: Processing chain to obtain an output file in standard format from different input datasets.

To evaluate the results of the estimation methods from a quantitative point of view, we have chosen the statistical parameters described in section 2.4. Once the statistics for each pair of methods have been computed, we generate tables with that information in order to facilitate the method evaluation. Furthermore, to help result interpretation we generate arrow images to visualize the estimated flow. In the case we know the optic flow groundtruth, we also generate a binary image which provides information about the method that performs better at each pixel, so it is very easy to identify the areas where one method outperforms another. This is very interesting because it provides very useful information for designing new methods in the future.

The following sections describe in a further detail some critical points concerning this methodology that have been discussed by all the partners involved on the FLUID project.

2.1 Input Data

The FLUID partners have provided some synthetic and real datasets in TIF format with the aim of studying optic flow estimators in the context of fluid image sequences. Synthetic datasets describe theoretical motion where the groundtruth flow is known, which allow us to provide quantitative error measures. It is desirable that these synthetic datasets describe realistic fluid motion in order to achieve the main goal of this project.

Real data is also provided to validate the conclusions in the real world. In this case, the groundtruth motion vector field is not given, so it is not possible to obtain an error clasification, but we are able to evaluate the different estimations among them to conclude if two methods provide similar responses.

Currently, the database provided by all the partners in the FLUID web site consists of the following elements:

- **Synthetic and Real PIV Datasets (Pckg-1):** Several datasets with real and synthetic PIV images provided by AEROBIO-CEMAGREF. These datasets are described on [1]. In our experiments we will use slices 23 and 24.
- **Synthetic PIV Dataset (Pck-4):** A pair of synthetic test images provided by LaVision, completely described in [2].
- **Synthetic 3D PIV Dataset (Pck-6):** A synthtetic dataset provided by LaVision with 3D motion in PIV volumes, as it is described in [3].
- **Real MSG Dataset (Pck-2 and Pck-5):** A complete dataset of MSG images provided by Laboratoire de Météorologie Dynamique, completely described in [4]. The dataset provided in **Pck-5** extends the one in **Pck-2**. In our experiments we use slices 48 and 49.
- **Real PIV Dataset (Pck-3):** A sequence of 100 real PIV images provided by LaVision. In our experiments we use slices 48 and 49.

2.2 Optic Flow Methods

The main goal of this paper is to explore the behaviour of a standard computer vision approaches to the problem of fluid optic flow estimation. To fit ideas, in this report we are going to use 4 different methods based either on Partial Differential Equations (PDE), Correlation (COR) or Structure Tensor (STE), as it is explained below:

- **PDE - Simple Flow (SF):** This variational approach minimizes the energy function in Eq. 1, where $\overline{h}$ is the motion vector we want to estimate, $I_i, i = \{1, 2\}$ are the input images, $D(\nabla I_1)$ is a regularized projection matrix in the direction perpendicular to ∇I_1 and C a weighting function:

$$E(\overline{h}) = \int_\Omega (I_1(\overline{x}) - I_2(\overline{x} + \overline{h}))^2 dx + C \int_(\Omega) trace((\nabla \overline{h}^T) D(\nabla I_1)(\nabla \overline{h}))dx \quad (1)$$

- **PDE - Video Flow (VD):** This method is also based on PDE, but uses at least three input images to estimate the flow. In this case, the solution is provided by the function $\overline{h}$ that minimizes this energy function:

$$\begin{aligned} E(\overline{h}) = \sum_{i=1}^{N-1} \int_\Omega (I_i(\overline{x}) - I_{i+1}(\overline{x} + \overline{h}_i))^2 dx + \\ C \sum_{i=1}^{N-1} \int_\Omega trace(\nabla \overline{h}^T D(\nabla I_i) \nabla \overline{h}_i^T) dx \\ +D \sum_{i=1}^{N-2} \int_(\Omega) \Phi(\| \overline{h}_i - \overline{h}_{i+1}(\overline{x} + \overline{h}_i) dx \end{aligned} \quad (2)$$

- **Correlation (COR):** We also use a correlation method to estimate the optical flow. The correlation function $C(x', y')$ in Eq. 3 provides a similarity criterion to compare two images within a given domain W, since the points (x', y') where $C(x', y')$ attains its maximum in W provides an estimation of the flow $\overline{h} = (x' - x, y' - y)$.

$$C(x', y') = \int_W I_1(x + l, y + m) I_2(x' + l, y' + m) dldm \quad (3)$$

- **Structure Tensor (STE):** This method is based in a multiscale comparison of the information provided by the structure tensor at different scales with the following similarity criterion:

$$D_{ste}(x,y,x',y') = \sum_1^N \omega_{i,0}|I_1^{\sigma_i}(x,y) - I_2^{\sigma_i}(x',y')| +$$
$$\sum_1^N \omega_{i,1}|\lambda_{min}^{1,\sigma_i}(x,y) - \lambda_{min}^{2,\sigma_i}(x',y')| + \sum_1^N \omega_{i,2}|\lambda_{max}^{1,\sigma_i}(x,y) - \lambda_{max}^{2,\sigma_i}(x',y')| +$$
$$\sum_1^N \omega_{i,3}| < \bar{e}_{max}^{1,\sigma_i}(x,y) - \bar{e}_{max}^{2,\sigma_i}(x',y') > - \overline{< \bar{e}_{max}^{1,\sigma_i}(x,y) - \bar{e}_{max}^{2,\sigma_i}(x',y') >}| \quad (4)$$

  where $\lambda_k^{l,\sigma_i}, l = \{1,2\}, k = \{min, max\}$ define the minimum or maximum eigenvalues of the $l-th$ image at scale σ_i, $\bar{e}_k^{l,\sigma_i}, l = \{1,2\}, k = \{min, max\}$ define the associated eigenvectors to either the maximum or minimum eigenvalues of the $l-th$ image at scale σ_i and $\omega_{i,j}$ are weighting parameters for each term.

For a further description of these estimators and details of their implementation, we refer the reader to [5] and [6].

Concerning the methods based on PDE's the CVGPR group has developed a library to perform a multiscale motion estimation analysis of image sequences [7]. The aim of this work is to compare different regularization terms in global variational approaches in order to study the contribution of this term to the final result in the context of fluid motion and with the fixed data term detailed in [8].

2.3 Output Data

All the methods detailed in the previous section provide the estimated flow in a standard file format in order to be able to share those results with other FLUID partners and to be able to evaluate different motion estimators. The standard file format is the following:

```
# Filename.txt
# Comments on the results:
# Results generated on 20th December 2005.

# Method: PDE - Simple Flow.
# Parameters to generate these results:
# Parameter_name 1: 5
# Parameter_name 2: 33
# ...
# Parameter_name N: 7
# Results:
1024 1024
0 0 1 1
0 1 1 1
...
1023 1022 2 1
1023 1023 1 0
```

Lines starting with symbol # are considered as comments with the aim to give all the necessary information about the current results. We suggest to write here the method used to compute the flow and all the parameter values that are necessary. Then, the first line after the comment area provides two numbers corresponding to the width and height of input images.

Finally, four numbers separated by blank spaces are written to represent the flow information using the following pattern:

```
i j u v
```

where the pair (i, j) indicates the position on the dense grid using the reference system shown in Fig. 2, where the origin $(0, 0)$ is on the left bottom part of the image. The pair (u, v) represent respectively the horizontal and vertical components of the estimated motion vector field, also relative to the same reference system shown in Fig. 2.

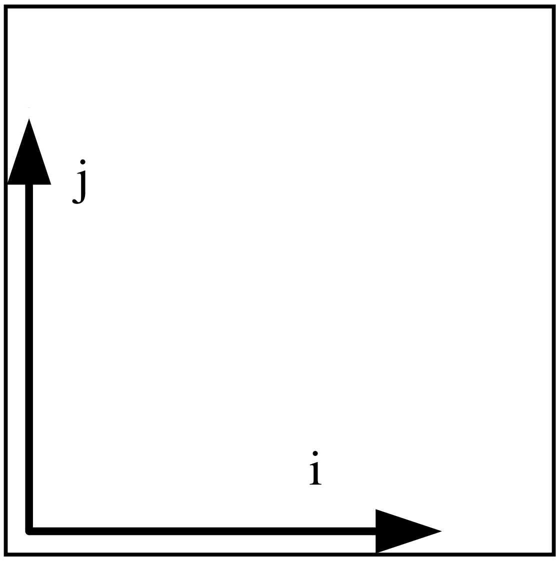

Figure 2: Reference system used to compute the results.

2.4 Error Measures

2.4.1 Quantitative Measures

In order to validate the results obtained with the methods under study, we compute the following statistical quality indicators which provide a scalar error measure:

- **angular error**: average difference between the angles of collocated vectors (in degrees):

$$\psi E = \frac{180}{N\pi} \sum_{i=1}^{N} \arccos(\overline{h}_i \cdot \overline{h}_{ref\ i}) \tag{5}$$

- **bias**: average difference between the amplitude or speed of collocated vectors:

$$BIAS = \frac{1}{N} \sum_{i=1}^{N} (\|\overline{h}_i\| - \|\overline{h}_{ref\ i}\|) \tag{6}$$

- **RMS vector difference (RMSVD), sometimes called RMS error**: average vector difference between collocated vectors:

$$RMSVD = \frac{1}{N} \sum_{i=1}^{N} \|\overline{h}_i - \overline{h}_{ref\ i}\| \tag{7}$$

- **normalized RMS vector difference (NRMSVD), sometimes called normalized RMS error**: with values between 0 and 1, average vector difference between collocated vectors divided by the average amplitude or speed of the vectors of the reference field:

$$NRMSVD = \frac{RMSVD}{\frac{1}{N}\sum_{i=1}^{N} \|\overline{h}_{ref\ i}\|} = \frac{\left\|\sum_{i=1}^{N} \overline{h}_i - \overline{h}_{ref\ i}\right\|}{\sum_{i=1}^{N} \|\overline{h}_{ref\ i}\|} \tag{8}$$

with N: number of collocated vectors, $\overline{h}_i$: i-th motion vector of the tested field, $\overline{h}_{ref\ i}$: i-th motion vector of the reference field.

In the case the groundtruth solution is not known the above statistics allow us to classify the methods following the result similarity.

2.4.2 Qualitative Measures

In addition to statistical error measures, a qualitative analysis of the results is also carried out. When the groundtruth motion vector field is given, for instance when we work with synthetic datasets, a binary image is built where each pixel colour represents the method that provides a more accurate result at that pixel. In this way, we are able to identify the areas in the image where one method performs better than the other

However, if the groundtruth is not known, the qualitative comparison is carried out drawing the vector fields provided by all the methods using an arrow representation with different colours for each one. In this way, it is easy to have a global overview of all the estimations.

3 Results

In this section we present the results we obtain when comparing the four methods outlined in section 2.2 using the methodology proposed in this paper. In this way, for each statistical parameter we present a table with the results for each pair of estimated motion vectors provided by either Simple Flow (SF), Video Flow (VD), correlation (COR) or structure tensor (STE) based approach and also with the groundtruth solution (TRUE) when it is known.

3.1 Synthetic PIV datasets:

3.1.1 Uniform Flow:

Tables from 1 to 4 show a statistical analysis of the results obtained for the uniform flow. From these results it is clear that all the methods provide a good estimation since the error is quite similar and low in comparison with the grountruth solution.

Figure 3 compares the groundtruth vector field (represented in red) with the solution provided by the correlation based method (represented in green), which provides the statistically best estimation. From the image, we can see that the main component of the error is found on the borders of the image.

BIAS	**TRUE**	**SF**	**VD**	**COR**	**STE**
TRUE	0.0000	-0.0333	-0.0599	0.0040	-0.0477
SF	0.0333	0.0000	-0.0266	0.0373	-0.0143
VD	0.0599	0.0266	0.0000	0.0640	0.0122
COR	-0.0040	-0.0373	-0.0640	0.0000	-0.0517
STE	0.0477	0.0143	-0.0122	0.0517	0.0000

Table 1: BIAS error for uniform flow

RMSVD	**TRUE**	**SF**	**VD**	**COR**	**STE**
TRUE	0.0000	0.0690	0.0970	0.0187	0.2372
SF	0.0690	0.0000	0.0827	0.0847	0.2069
VD	0.0970	0.0827	0.0000	0.1131	0.2260
COR	0.0187	0.0847	0.1131	0.0000	0.2483
STE	0.2372	0.2069	0.2260	0.2483	0.0000

Table 2: RMSVD error for uniform flow

NRMSVD	**TRUE**	**SF**	**VD**	**COR**	**STE**
TRUE	0.0000	0.0061	0.0086	0.0016	0.0210
SF	0.0061	0.0000	0.0073	0.0075	0.0183
VD	0.0086	0.0073	0.0000	0.0100	0.0201
COR	0.0016	0.0075	0.0100	0.0000	0.0220
STE	0.0211	0.0184	0.0201	0.0221	0.0000

Table 3: NRMSVD error for uniform flow

ANG. ERR.	**TRUE**	**SF**	**VD**	**COR**	**STE**
TRUE	0.0000	2.7036	3.6246	51.4173	36.8139
SF	2.7036	0.0000	2.9081	3.4390	10.8006
VD	3.6246	2.9081	0.0000	4.4152	12.1942
COR	51.4173	3.4390	4.4152	0.0000	37.9775
STE	36.8139	10.8006	12.1942	37.9775	0.0000

Table 4: Angular Error for uniform flow

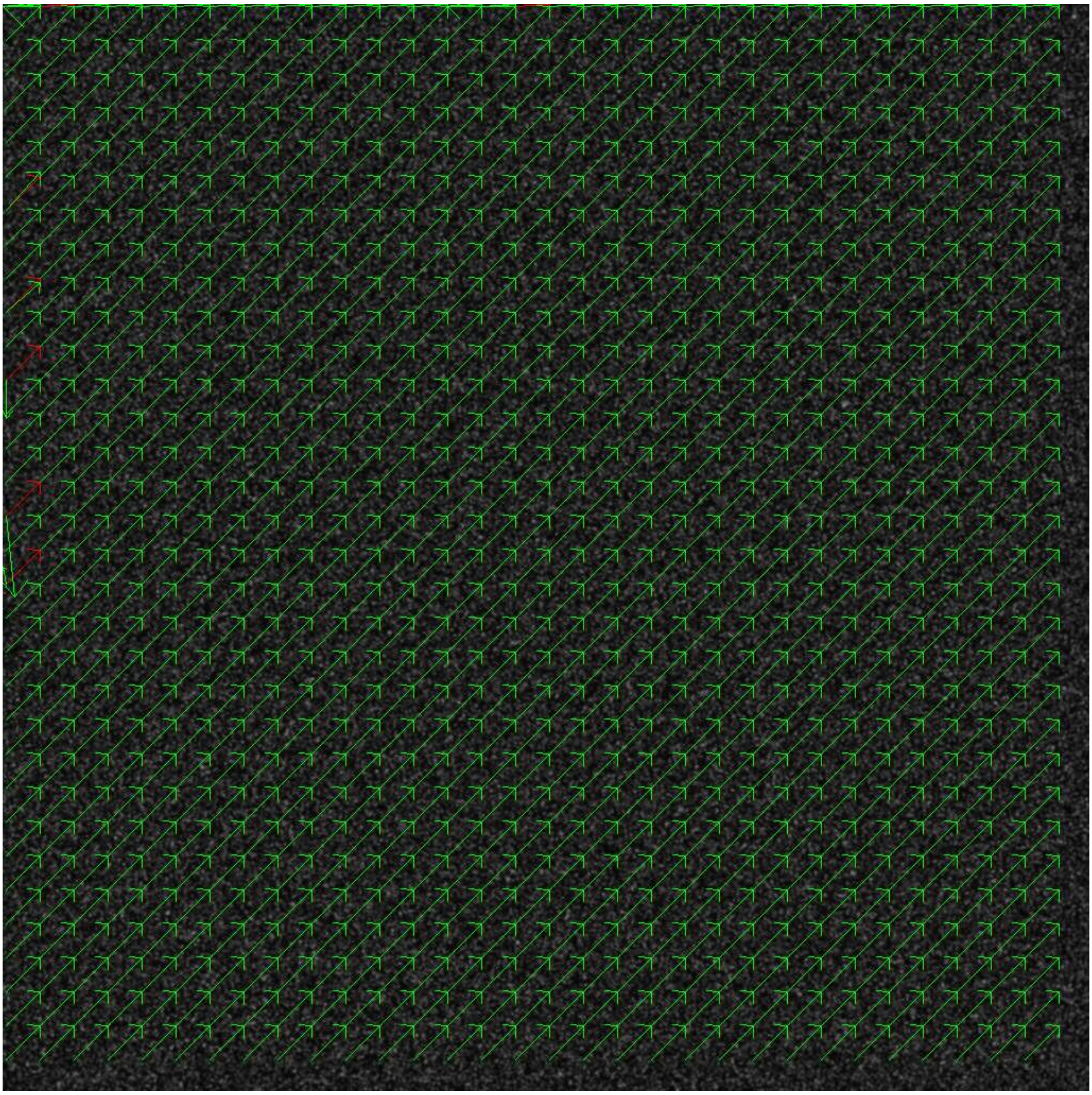

Figure 3: Estimated Vector Field for uniform flow. (Red: TRUE, Green: COR)

3.1.2 Poiseuille Flow:

Tables from 5 to 8 show a statistical analysis of the results obtained for the Poiseuille flow model. From these results we can also conclude that all the methods provide a good estimation since the error is quite similar and low in comparison with the grountruth solution.

Figure 4 compares the groundtruth vector field (represented in red) with the solution provided by the Simple Flow estimation method (represented in green), which provides the statistically best estimation. In this case, the main component of the error is found on the areas where the magnitude of the flow is small, that is, on top and bottom of the image.

BIAS	TRUE	SF	VD	COR	STE
TRUE	0.0000	-0.0475	-0.0718	-0.0388	0.0154
SF	0.0475	0.0000	-0.0242	0.0087	0.0630
VD	0.0718	0.0242	0.0000	0.0329	0.0873
COR	0.0388	-0.0087	-0.0329	0.0000	0.0543
STE	-0.0154	-0.0630	-0.0873	-0.0543	0.0000

Table 5: BIAS error for Poiseuille model flow

RMSVD	TRUE	SF	VD	COR	STE
TRUE	0.0000	0.0748	0.0973	0.2911	0.5559
SF	0.0748	0.0000	0.0427	0.3265	0.5265
VD	0.0973	0.0427	0.0000	0.3456	0.5182
COR	0.2911	0.3265	0.3456	0.0000	0.4502
STE	0.5559	0.5265	0.5182	0.4502	0.0000

Table 6: RMSVD Error for Poiseuille model flow

NRMSVD	TRUE	SF	VD	COR	STE
TRUE	0.0000	0.0070	0.0091	0.0272	0.0519
SF	0.0070	0.0000	0.0040	0.0306	0.0494
VD	0.0091	0.0040	0.0000	0.0325	0.0487
COR	0.0273	0.0306	0.0324	0.0000	0.0422
STE	0.0519	0.0492	0.0484	0.0420	0.0000

Table 7: NRMSVD Error for Poiseuille model flow

ANG. ERR.	TRUE	SF	VD	COR	STE
TRUE	0.0000	0.4368	0.4697	1.2380	3.0357
SF	0.4368	0.0000	0.3730	1.2301	2.9845
VD	0.4697	0.3730	0.0000	1.2951	2.9996
COR	1.2380	1.2301	1.2951	0.0000	14.3772
STE	3.0357	2.9845	2.9996	14.3772	0.0000

Table 8: Angular Error for Poiseuille model flow

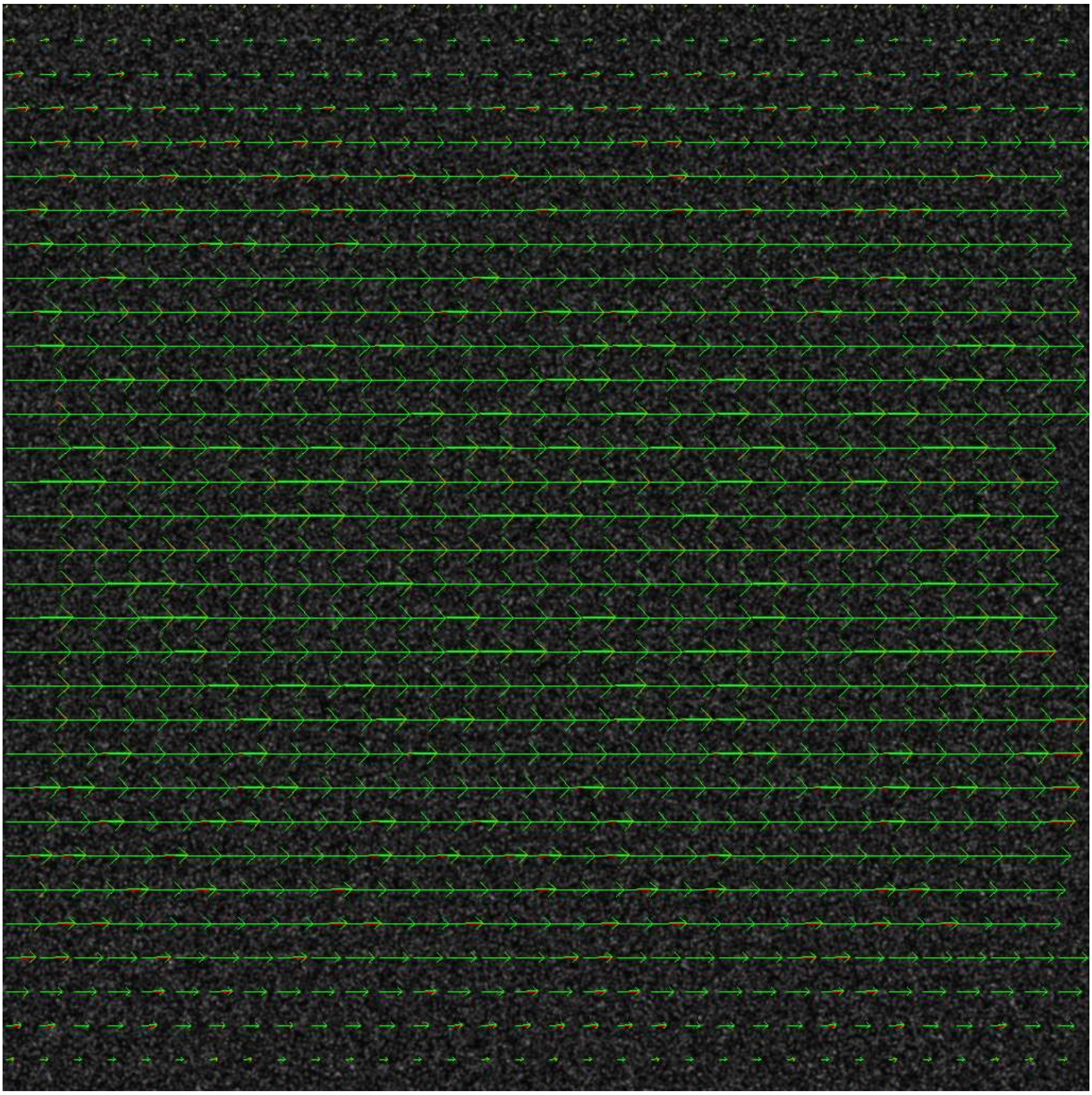

Figure 4: Estimated Vector Field for Poiseuille model flow. (Red: TRUE, Green: SF)

3.1.3 Lamb-Oseen model flow:

Tables from 9 to 12 show the statistical analysis of the results obtained for the Lamb-Oseen flow model, which is a bit more complex than the previous since it includes orientation variation of the motion vector field, not only magnitude variation. For this model, we can conclude that the Structure Tensor based approach provides the worst results, while the error for the others is quite similar and low in comparison with the groundtruth solution.

Figure 5 compares the groundtruth vector field (represented in red) with the solution provided by the correlation based approach (represented in green), which provides the statistically best estimation. In this case, the main error is found on the center of the image, where the orientation is not quite accurate.

BIAS	**TRUE**	**SF**	**VD**	**COR**	**STE**
TRUE	0.0000	-0.0165	-0.0193	-0.0508	-13.6123
SF	0.0165	0.0000	-0.0027	-0.0342	-13.5959
VD	0.0193	0.0027	0.0000	-0.0315	-13.5927
COR	0.0508	0.0342	0.0315	0.0000	-13.5577
STE	13.6123	13.5959	13.5927	13.5577	0.0000

Table 9: BIAS error for Lamb-Oseen model flow

RMSVD	TRUE	SF	VD	COR	STE
TRUE	0.0000	0.5773	1.5768	0.5066	18.1461
SF	0.5773	0.0000	1.0380	0.7731	18.1201
VD	1.5768	1.0380	0.0000	1.6685	18.1258
COR	0.5066	0.7731	1.6685	0.0000	18.0964
STE	18.1461	18.1201	18.1258	18.0964	0.0000

Table 10: RMSVD error for Lamb-Oseen model flow

NRMSVD	TRUE	SF	VD	COR	STE
TRUE	0.0000	0.0319	0.0872	0.0280	1.0041
SF	0.0319	0.0000	0.0574	0.0428	1.0035
VD	0.0873	0.0575	0.0000	0.0924	1.0041
COR	0.0281	0.0429	0.0926	0.0000	1.0053
STE	4.0763	4.0705	4.0718	4.0652	0.0000

Table 11: NRMSVD error for Lamb-Oseen model flow

ANG. ERR.	TRUE	SF	VD	COR	STE
TRUE	0.0000	1.8087	4.8995	1.3541	85.7099
SF	1.8087	0.0000	3.2106	2.2928	85.5922
VD	4.8995	3.2106	0.0000	5.1682	85.6596
COR	1.3541	2.2928	5.1682	0.0000	85.8962
STE	85.7099	85.5922	85.6596	85.8962	0.0000

Table 12: Angular Error for Lamb-Oseen model flow

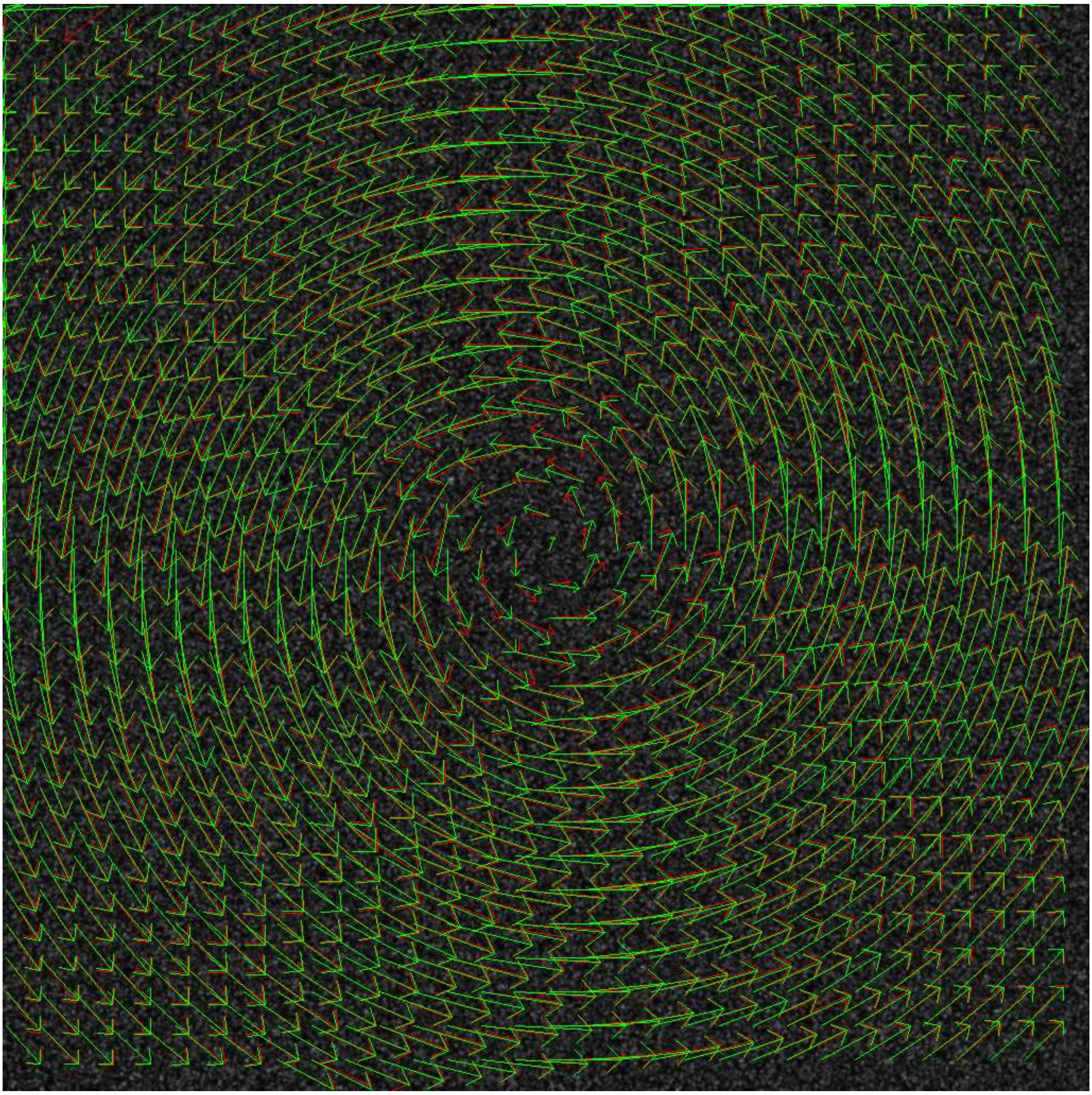

Figure 5: Estimated Vector Field for Lamb-Oseen model flow. (Red: TRUE, Green: COR)

3.1.4 Sink flow:

Tables from 13 to 16 show a statistical analysis of the results obtained for the sink flow model, which also includes orientation variation. For this model, we can also conclude that the Structure Tensor based approach does not perform quite well, while the error for the others is quite similar and low in comparison with the groundtruth solution.

Figure 4 compares the groundtruth vector field (represented in red) with the solution provided by the Simple Flow estimation method (represented in green), which provides the statistically best estimation. Again, the main error is found on the center of the image, where the orientation is not quite accurate.

BIAS	TRUE	SF	VD	COR	STE
TRUE	0.0000	-0.5562	-0.4019	-0.3894	-1.4786
SF	0.5562	0.0000	0.1531	0.1657	-0.9234
VD	0.4019	-0.1531	0.0000	0.0125	-1.0766
COR	0.3894	-0.1657	-0.0125	0.0000	-1.0892
STE	1.4786	0.9234	1.0766	1.0892	0.0000

Table 13: BIAS error for sink flow

RMSVD	TRUE	SF	VD	COR	STE
TRUE	0.0000	0.7274	0.9190	1.3919	2.2600
SF	0.7274	0.0000	0.2772	1.0196	1.6951
VD	0.9190	0.2772	0.0000	1.1515	1.8069
COR	1.3919	1.0196	1.1515	0.0000	1.7438
STE	2.2600	1.6951	1.8069	1.7438	0.0000

Table 14: RMSVD error for sink flow

NRMSVD	TRUE	SF	VD	COR	STE
TRUE	0.0000	0.1263	0.1596	0.2417	0.3925
SF	0.1398	0.0000	0.0532	0.1960	0.3258
VD	0.1716	0.0517	0.0000	0.2150	0.3374
COR	0.2599	0.1904	0.2150	0.0000	0.3256
STE	0.5297	0.3973	0.4235	0.4087	0.0000

Table 15: NRMSVD error for sink flow

ANG. ERR.	TRUE	SF	VD	COR	STE
TRUE	0.0000	0.5301	0.7422	5.4697	12.5471
SF	0.5301	0.0000	0.6971	5.4954	12.5748
VD	0.7422	0.6971	0.0000	5.5403	12.5942
COR	5.4697	5.4954	5.5403	0.0000	31.5669
STE	12.5471	12.5748	12.5942	31.5669	0.0000

Table 16: Angular Error for sink flow

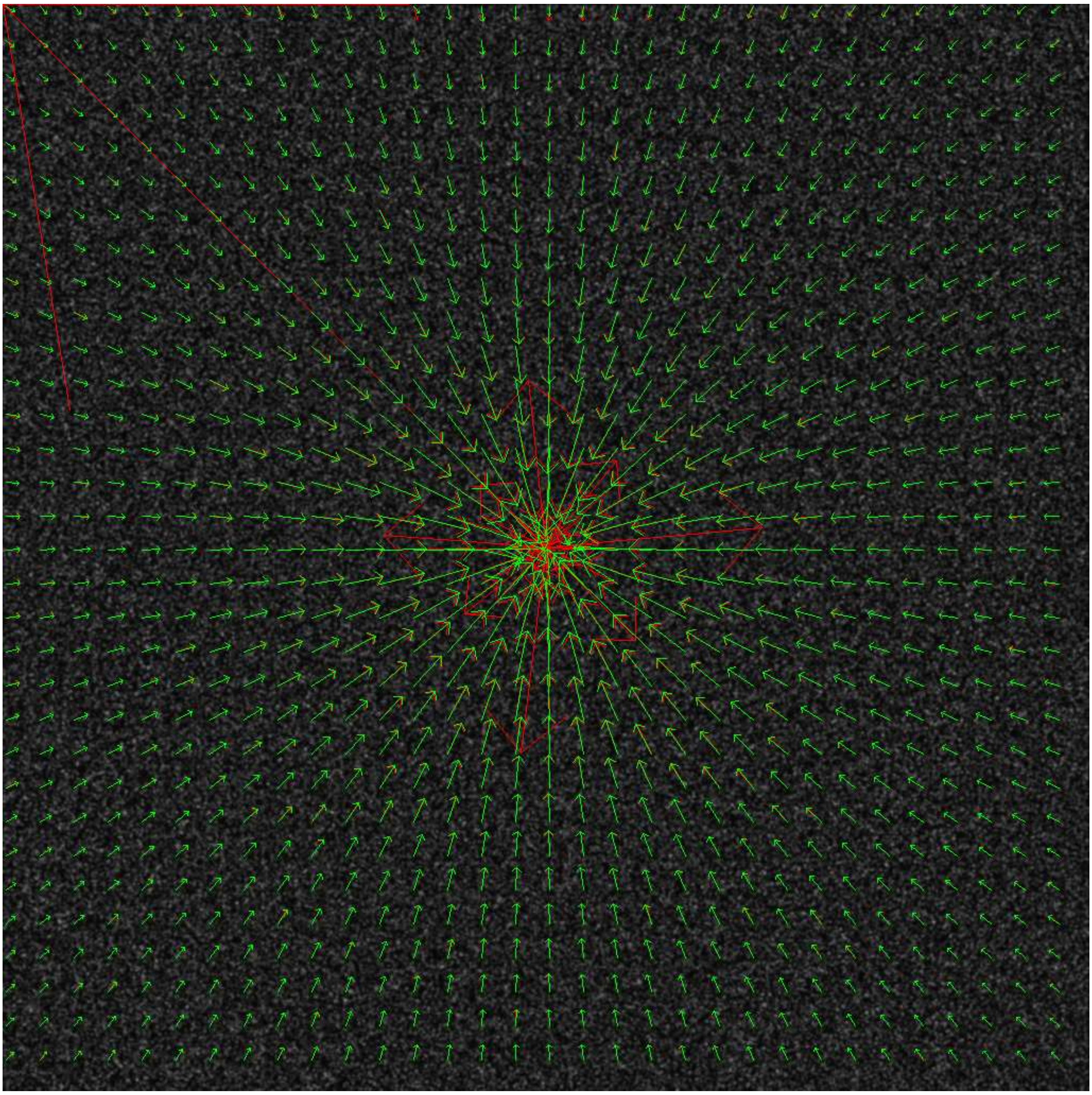

Figure 6: Estimated Vector Field for sink flow. (Red: TRUE, Green: SF)

3.1.5 Vortex flow:

Tables from 17 to 20 show a statistical analysis of the results obtained for the vortex flow model. In this case, we can also conclude that the Structure Tensor based approach does not perform quite well since the error measures indicate unaccurate results. On the other hand, the error measures for the other approaches are quite similar and low in comparison with the grountruth solution.

Figure 7 compares the groundtruth vector field (represented in red) with the solution provided by the Simple Flow estimation method (represented in green), which provides the statistically best estimation. Again, the main error is found on the center of the image, where neither the orientation nor the magnitude are very accurate.

BIAS	**TRUE**	**SF**	**VD**	**COR**	**STE**
TRUE	0.0000	-0.6207	-0.5007	-0.4241	-1.4934
SF	0.6207	0.0000	0.1192	0.1957	-0.8735
VD	0.5007	-0.1192	0.0000	0.0764	-0.9927
COR	0.4241	-0.1957	-0.0764	0.0000	-1.0693
STE	1.4934	0.8735	0.9927	1.0693	0.0000

Table 17: BIAS error for vortex flow

RMSVD	TRUE	SF	VD	COR	STE
TRUE	0.0000	0.7261	0.8925	1.3125	2.2338
SF	0.7261	0.0000	0.3549	0.9429	1.6276
VD	0.8925	0.3549	0.0000	1.0799	1.7515
COR	1.3125	0.9429	1.0799	0.0000	1.6819
STE	2.2338	1.6276	1.7515	1.6819	0.0000

Table 18: RMSVD error for vortex flow

NRMSVD	TRUE	SF	VD	COR	STE
TRUE	0.0000	0.1261	0.1550	0.2279	0.3879
SF	0.1413	0.0000	0.0690	0.1835	0.3167
VD	0.1697	0.0675	0.0000	0.2054	0.3331
COR	0.2465	0.1771	0.2029	0.0000	0.3160
STE	0.5253	0.3827	0.4118	0.3955	0.0000

Table 19: NRMSVD error for vortex flow

ANG. ERR.	TRUE	SF	VD	COR	STE
TRUE	0.0000	1.1086	2.3488	5.1137	12.4459
SF	1.1086	0.0000	1.8249	5.3256	12.3912
VD	2.3488	1.8249	0.0000	5.9060	12.5472
COR	5.1137	5.3256	5.9060	0.0000	30.5896
STE	12.4459	12.3912	12.5472	30.5896	0.0000

Table 20: Angular Error for vortex flow

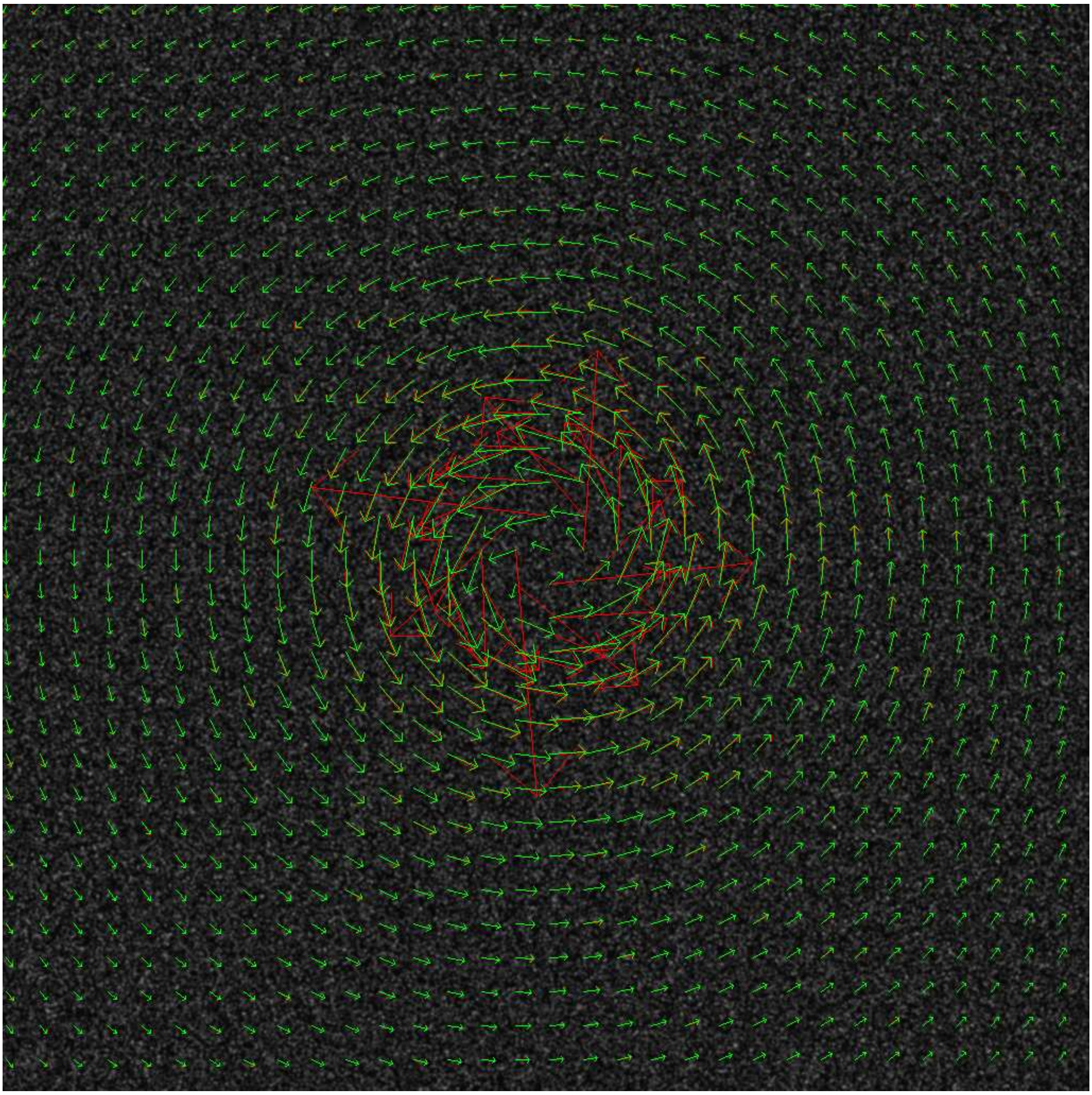

Figure 7: Estimated Vector Field for vortex flow. (Red: TRUE, Green: SF)

3.1.6 Cylinder with Γ:

Tables from 21 to 24 show a statistical analysis of the results obtained for the flow model around a Cylinder. In this case, we can also conclude that the Structure Tensor based approach does not perform quite well since the error measures indicate unaccurate results. Again, the error measures for the other approaches are quite similar and low in comparison with the grountruth solution.

Figure 8 compares the groundtruth vector field (represented in red) with the solution provided by the Simple Flow estimation method (represented in green), which provides the statistically best estimation. In this case, the error is mainly found around the cylinder, where the magnitude of the flow is higher. In addition, we detect some flow inside the cylinder where there should not be any.

BIAS	TRUE	SF	VD	COR	STE
TRUE	0.0000	-0.2436	0.1458	-0.1262	-1.9603
SF	0.2436	0.0000	0.3895	0.1174	-1.7167
VD	-0.1458	-0.3895	0.0000	-0.2721	-2.1062
COR	0.1262	-0.1174	0.2721	0.0000	-1.8342
STE	1.9603	1.7167	2.1062	1.8342	0.0000

Table 21: BIAS error for flow around a cylinder

RMSVD	TRUE	SF	VD	COR	STE
TRUE	0.0000	0.5362	0.5970	0.6705	3.6142
SF	0.5362	0.0000	0.6278	0.8064	3.2856
VD	0.5970	0.6278	0.0000	0.9371	3.6416
COR	0.6705	0.8064	0.9371	0.0000	3.3878
STE	3.6142	3.2856	3.6416	3.3878	0.0000

Table 22: RMSVD error for flow around a cylinder

NRMSVD	TRUE	SF	VD	COR	STE
TRUE	0.0000	0.0609	0.0678	0.0761	0.4105
SF	0.0626	0.0000	0.0733	0.0942	0.3839
VD	0.0667	0.0701	0.0000	0.1047	0.4069
COR	0.0772	0.0929	0.1079	0.0000	0.3903
STE	0.5286	0.4806	0.5327	0.4955	0.0000

Table 23: NRMSVD error for flow around a cylinder

ANG. ERR.	TRUE	SF	VD	COR	STE
TRUE	0.0000	2.2640	2.9397	3.9649	18.0253
SF	2.2640	0.0000	1.4110	4.0206	17.2016
VD	2.9397	1.4110	0.0000	4.4613	17.2733
COR	3.9649	4.0206	4.4613	0.0000	28.7393
STE	18.0253	17.2016	17.2733	28.7393	0.0000

Table 24: Angular Error for flow around a cylinder

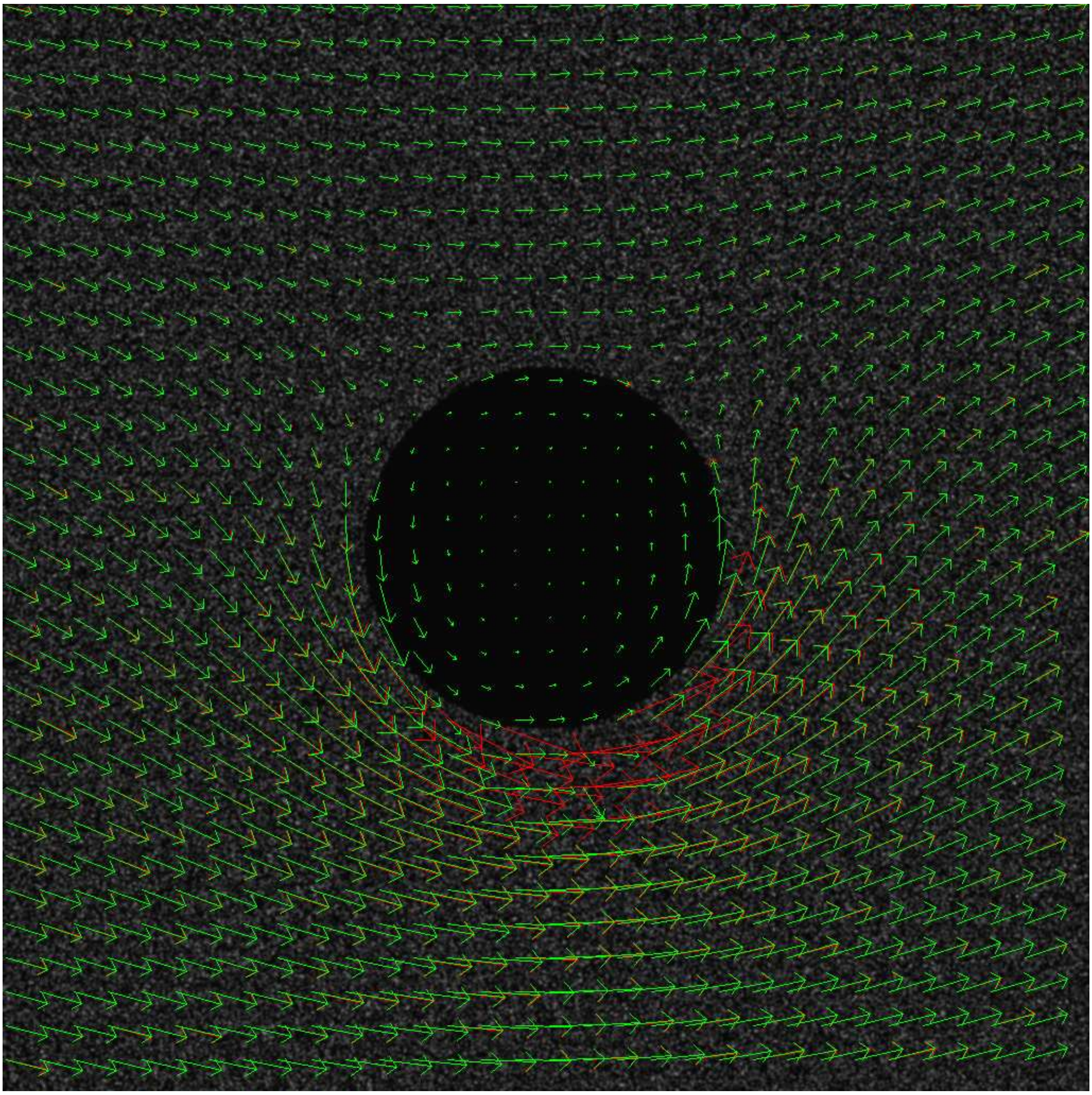

Figure 8: Estimated Vector Field for the flow around a cylinder. (Red: TRUE, Green: SF)

3.1.7 LaVision Test Images (PIV Challenge 2005):

Tables from 25 to 28 show a statistical analysis of the results obtained for the tests images provided by LaVision from PIV Challenge 2005. For this pair of images, we compare the best estimation obtained by LaVision (LAV), the Simple Flow (SF) scheme, our simple implementation of the correlation based approach (COR) and the structure tensor based approach (STE). In this case we are not able to use Video Flow (VD) approach because only two images have been provided. Again, the latter approach provides the highest error measures which indicate an unaccurate behaviour. The statistically best solution is that provided by LaVision, although Simple Flow or Correlation based approach also provide accurate results.

Figure 9 shows the estimated motion vector fields (represented in green (LAV), dark blue (SF) and light blue (STE)) and the groundtruth (represented in red). Since correlation and simple flow schemes provide quite similar responses we only represent the results provided by the latter in order to be able to distinguish different flows. Figures 10 and 11 show two selections of that image in order to visualize the details. As it can be seen, the structure tensor based approach detects some high and disoriented flow in areas where no motion is present. This problem also arises with the simple flow approach, but the detected flow is quite small and smooth. From 11, it can be seen that small 2D-sinusoidal motion is not accurately detected by any method.

BIAS	TRUE	LAV	SF	COR	STE
TRUE	0.0000	-0.0133	-0.0488	0.1684	1.2429
LAV	0.0133	0.0000	-0.0354	0.1818	1.2562
SF	0.0488	0.0354	0.0000	0.2172	1.2914
COR	-0.1684	-0.1818	-0.2172	0.0000	1.0759
STE	-1.2429	-1.2562	-1.2914	-1.0759	0.0000

Table 25: Bias error on the synthetic test image provided by LaVision (PIV Challenge 2005)

RMSVD	TRUE	LAV	SF	COR	STE
TRUE	0.0000	0.1962	0.4850	0.8274	2.3496
LAV	0.1962	0.0000	0.3971	0.8226	2.3415
SF	0.4850	0.3971	0.0000	0.8917	2.3592
COR	0.8274	0.8226	0.8917	0.0000	2.6084
STE	2.3496	2.3415	2.3592	2.6084	0.0000

Table 26: RMSVD error on the synthetic test image provided by LaVision (PIV Challenge 2005)

NRMSVD	TRUE	LAV	SF	COR	STE
TRUE	0.0000	0.1351	0.3340	0.5698	1.6181
LAV	0.1364	0.0000	0.2760	0.5718	1.6275
SF	0.3455	0.2829	0.0000	0.6353	1.6808
COR	0.5104	0.5074	0.5501	0.0000	1.6091
STE	0.8709	0.8679	0.8744	0.9668	0.0000

Table 27: NRMSVD error on the synthetic test image provided by LaVision (PIV Challenge 2005)

ANG. ERR.	TRUE	LAV	SF	COR	STE
TRUE	0.0000	6.6878	15.3600	22.6291	49.7657
LAV	6.6878	0.0000	12.6030	20.0793	47.4122
SF	15.3600	12.6030	0.0000	21.4572	46.8281
COR	22.6291	20.0793	21.4572	0.0000	60.7473
STE	49.7657	47.4122	46.8281	60.7473	0.0000

Table 28: Angular error on the synthetic test image provided by LaVision (PIV Challenge 2005)

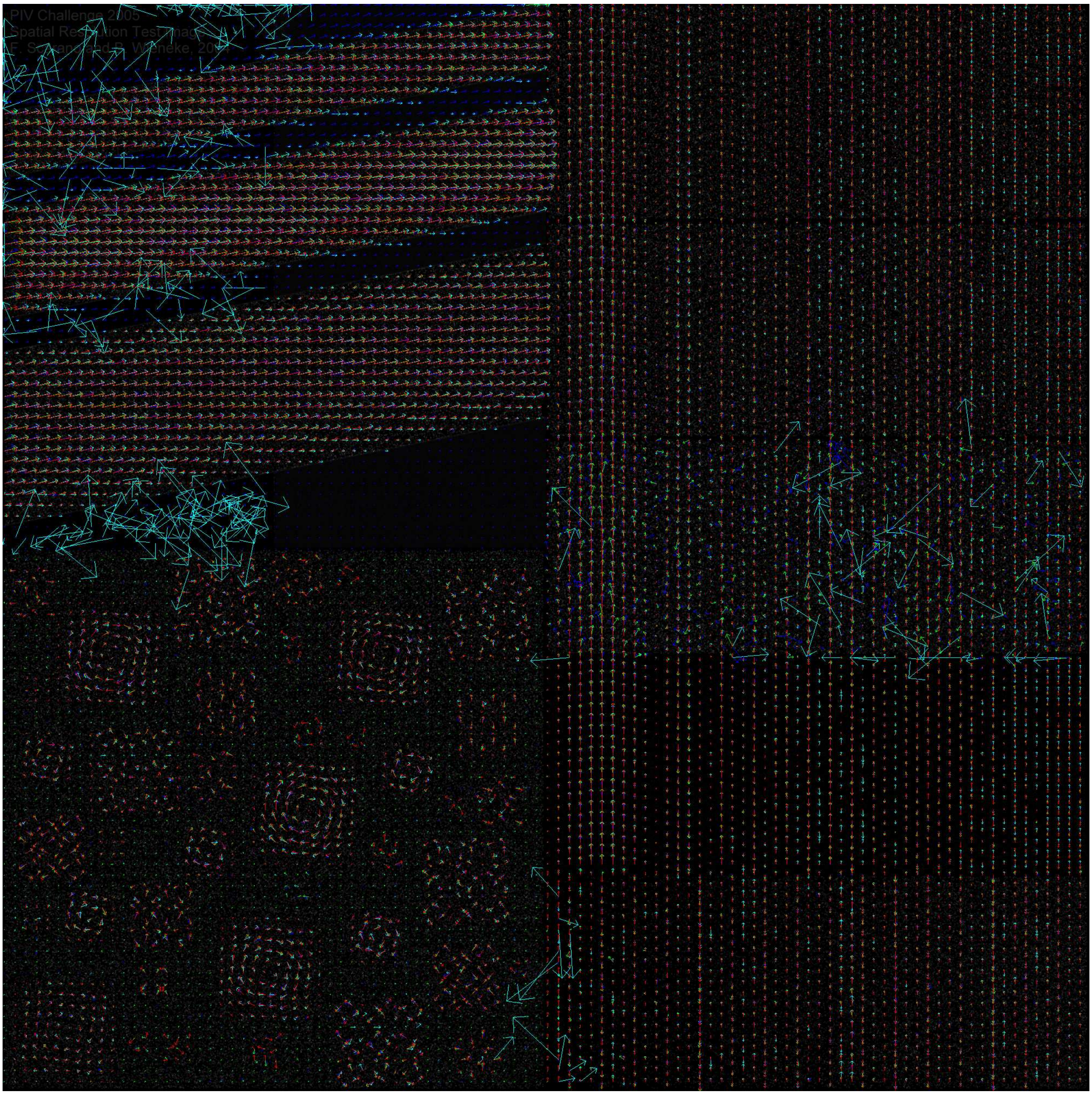

Figure 9: Estimated motion vector fields for the LaVision sequence (PIV Challenge 2005). (Red: TRUE, Green: LAV, Dark Blue: SF, Light Blue: STE)

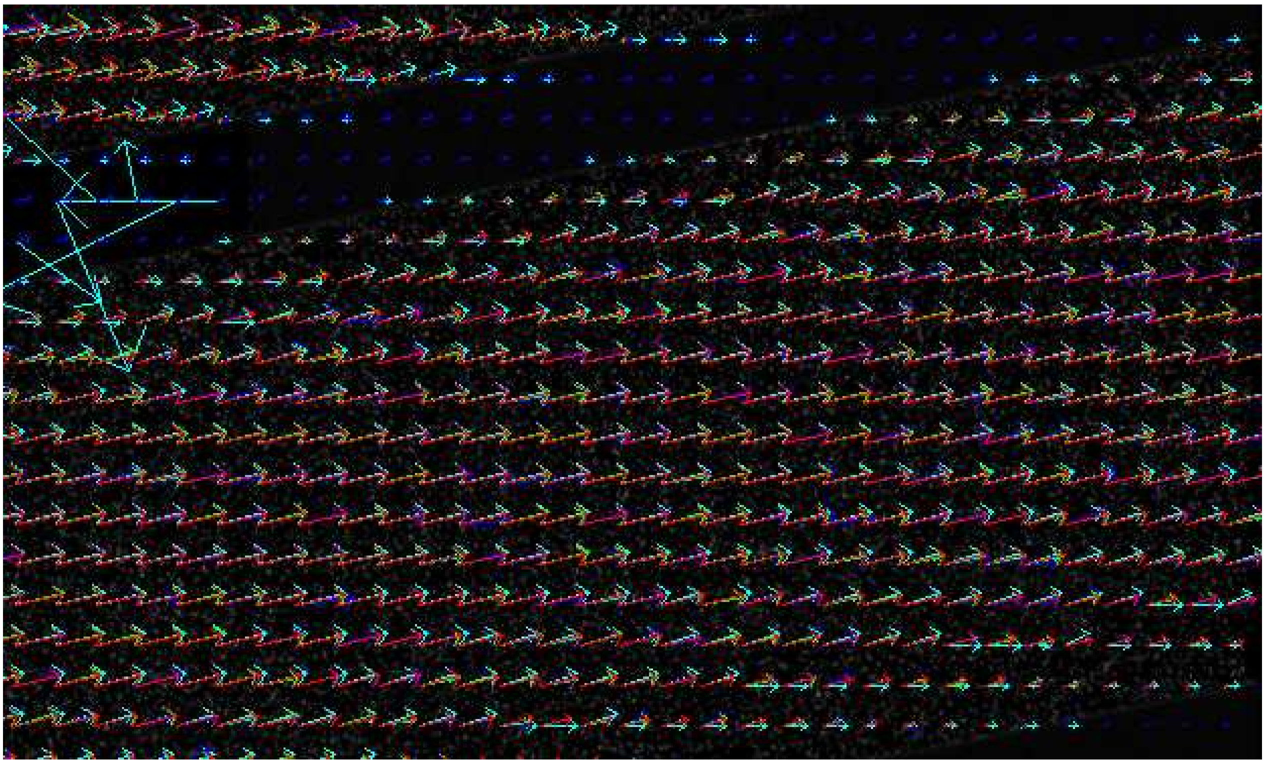

Figure 10: Selection on the Synthetic PIV image provided by LaVision (PIV Challenge 2005)

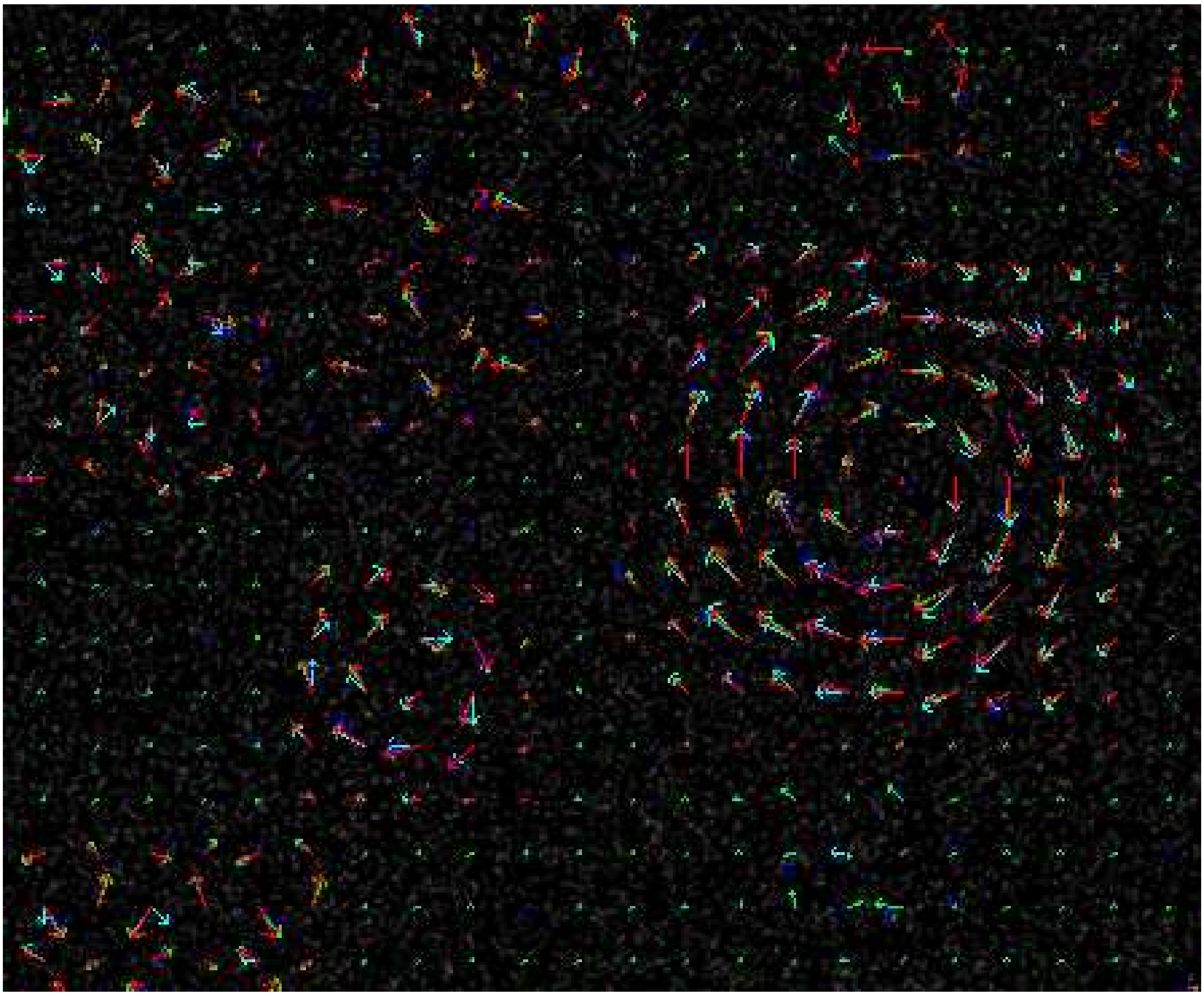

Figure 11: Selection on the Synthetic PIV image provided by LaVision (PIV Challenge 2005)

3.2 Real PIV datasets:

Once we have studied the flow with synthetic images, we would like to validate the main conclusions obtained for those simple flows with real datasets. In this case, we have the main concern in the fact that we cannot compare the responses with a groundtruth vector field since it remains unknown. The following sections present the results obtained for each dataset used in our experiments.

3.2.1 Wake Behind a Cylinder

Tables from 29 to 32 show a statistical analysis of the results obtained for the wake image sequence. In this case, we only compare simple flow (SF), correlation-based approach (COR) and structure tensor scheme (STE) since the sequence is taken in series of two consecutive image, but there is no time correlation between a pair of images and the following. Hence, the video flow approach (VD) cannot be applied. From the tables, we can also conclude that the STE method still provides less accurate results.

This is clearly seen on the images from 12 to 14, where it can be seen that the response from the structure tensor approach does not contain accurate information while those provided by the other methods are quite similar.

BIAS	**SF**	**COR**	**STE**
SF	0.0000	0.0697	2.8369
COR	-0.0697	0.0000	2.7671
STE	-2.8369	-2.7671	0.0000

Table 29: Bias error on the wake sequence

RMSVD	**SF**	**COR**	**STE**
SF	0.0000	0.4539	6.2230
COR	0.4539	0.0000	6.2491
STE	6.2230	6.2491	0.0000

Table 30: RMSVD error on the wake sequence

NRMSVD	**SF**	**COR**	**STE**
SF	0.0000	0.1510	2.0702
COR	0.1476	0.0000	2.0318
STE	1.0651	1.0695	0.0000

Table 31: NRMSVD error on the wake sequence

ANGULARERROR	**SF**	**COR**	**STE**
SF	0.0000	7.1652	78.9412
COR	7.1652	0.0000	79.5506
STE	78.9412	79.5506	0.0000

Table 32: Angular error on the wake sequence

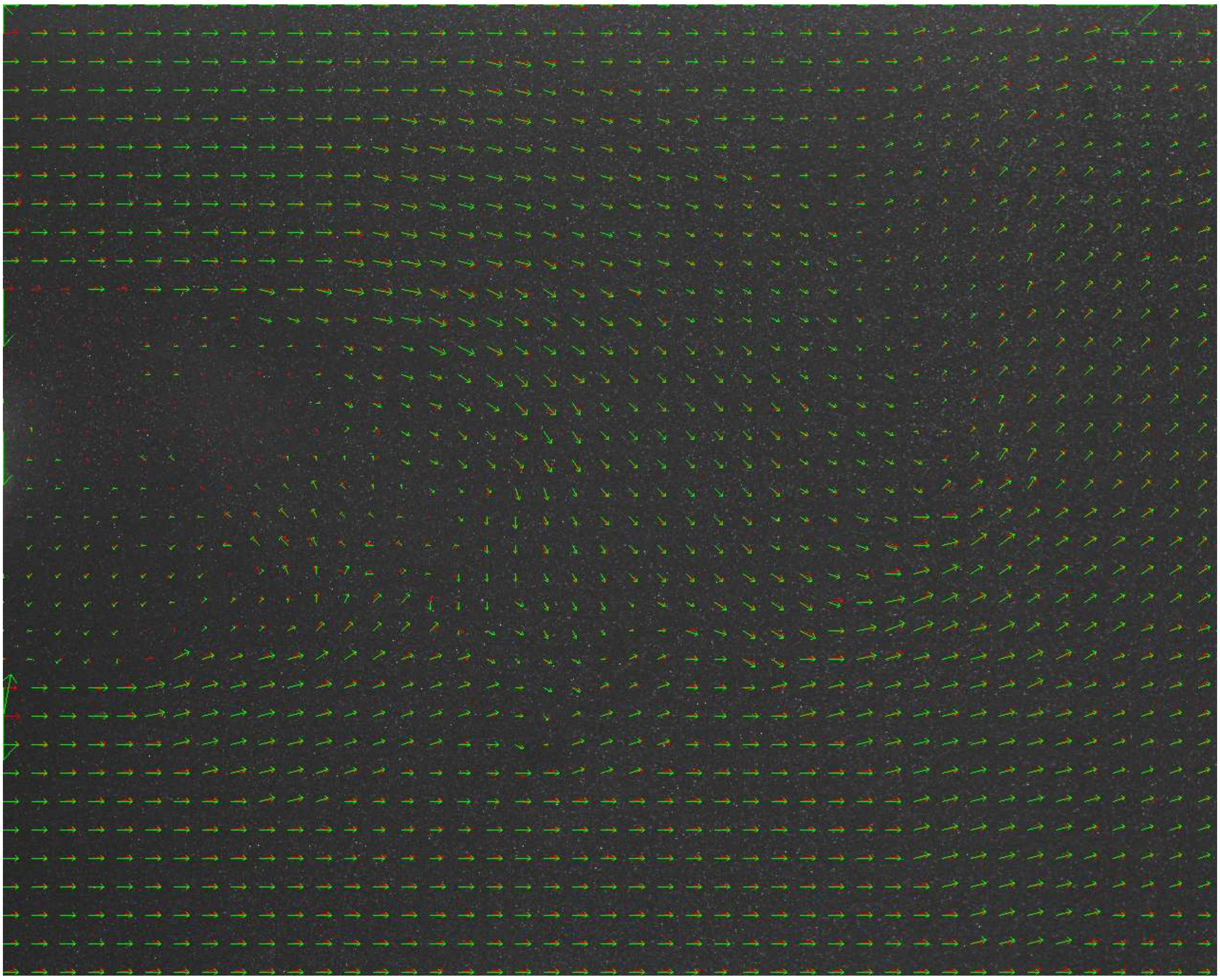

Figure 12: Estimated flow on the real PIV wake sequence (Red: SF, Green: COR)

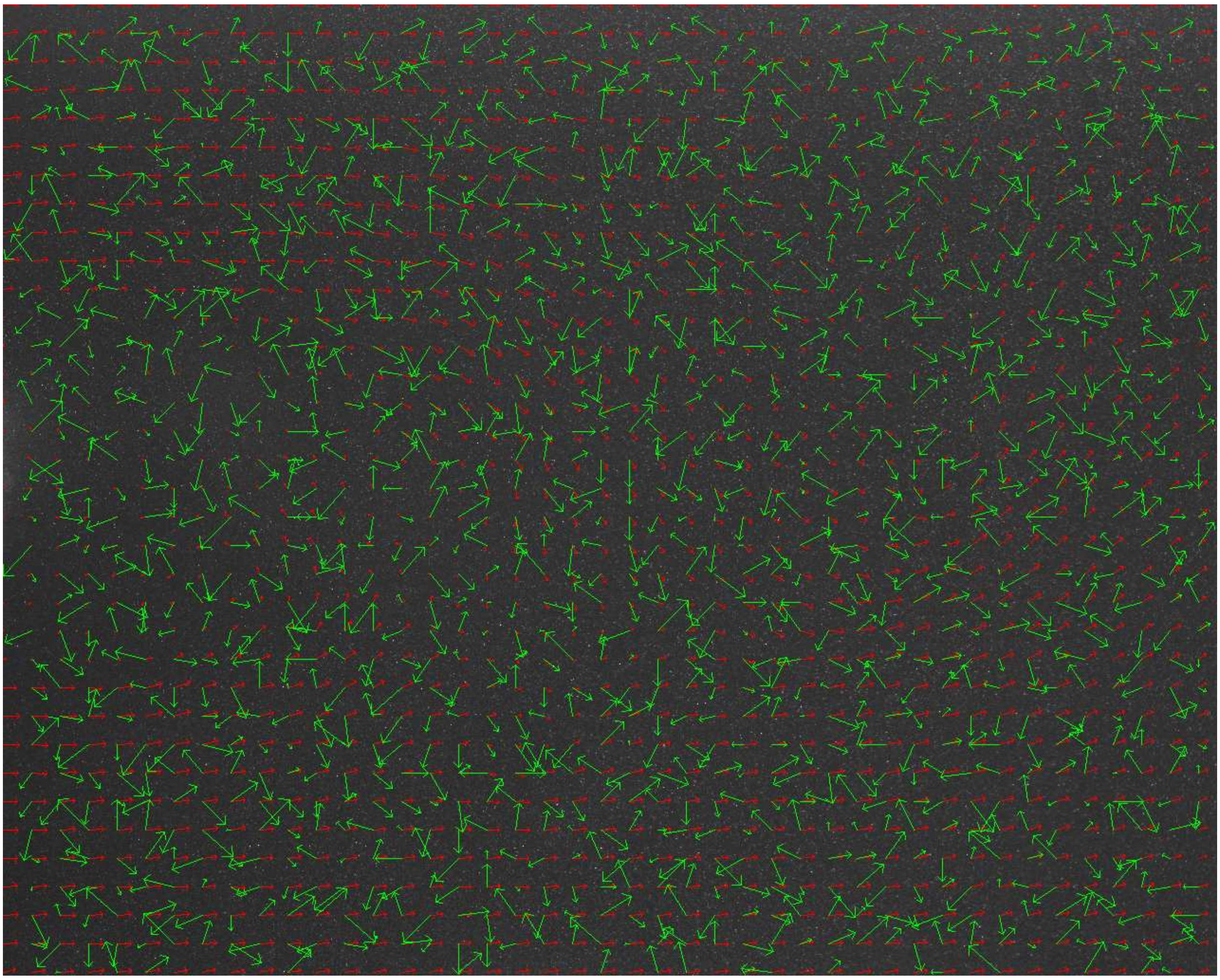

Figure 13: Estimated flow on the real PIV wake sequence (Red: SF, Green: STE)

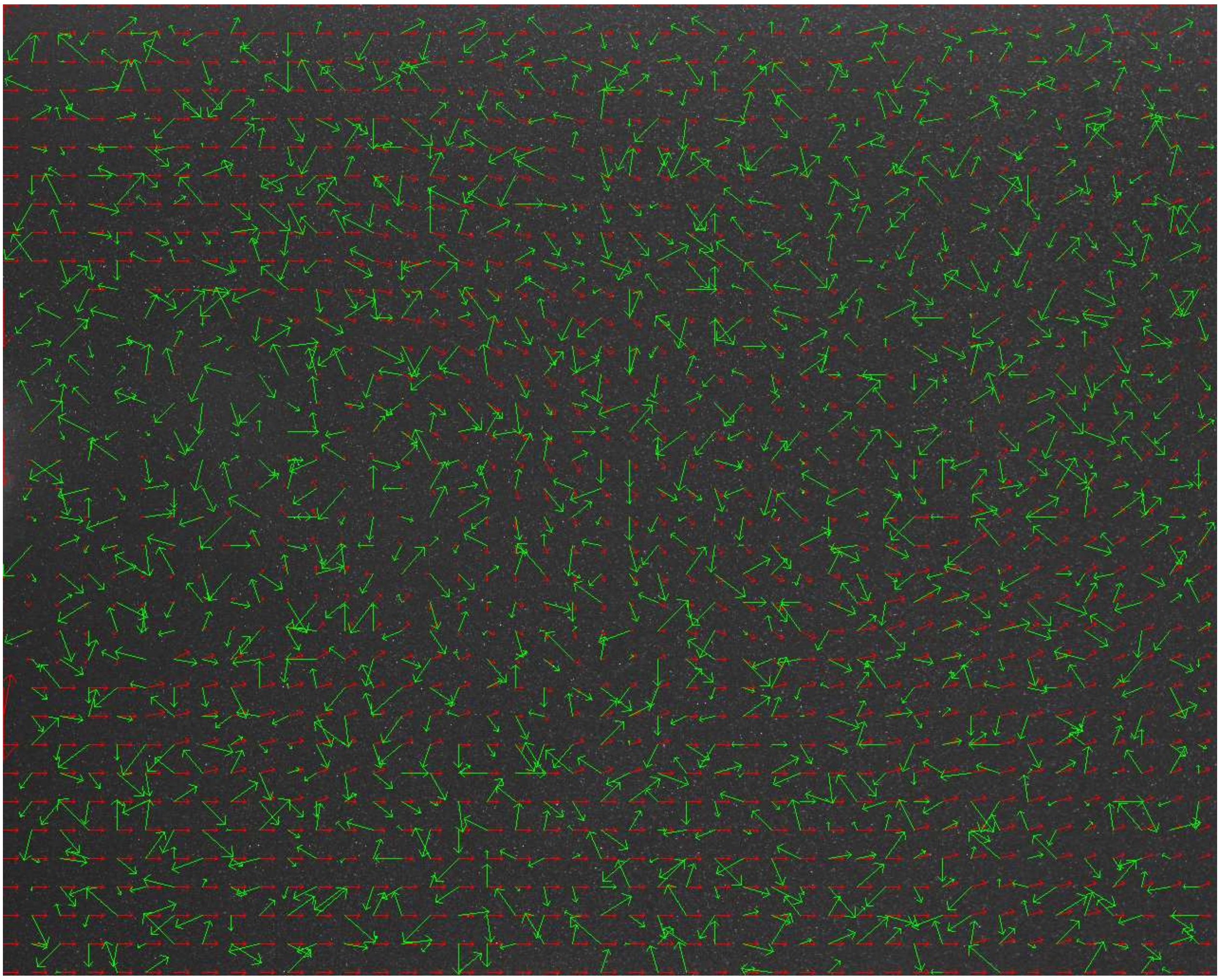

Figure 14: Estimated flow on the real PIV wake sequence (Red: COR, Green: STE)

3.2.2 Turbulent Air Flow:

Tables from 33 to 36 show a statistical analysis of the results obtained for the turbulent air image sequence. In this case, we can also see that the error from the structure tensor approach (STE) is larger in comparison to the other approaches, so we can conclude that its response may not be very accurate.

Figures 15 to 17 compare the approaches which provide similar responses in order to visualize where the main differences arise. In Fig. 15 and 16 we can clearly see that the response using PDE provides a smoothed motion vector field, while the correlation detects better areas where motion is not present. However, the correlation approach provides very large displacement vectors near boundaries.

BIAS	**SF**	**VD**	**COR**	**STE**
SF	0.0000	-0.3695	0.0382	-5.0886
VD	0.3695	0.0000	0.4077	-4.7191
COR	-0.0382	-0.4077	0.0000	-5.1267
STE	5.0886	4.7191	5.1267	0.0000

Table 33: Bias error on the turbulent air sequence

RMSVD	**SF**	**VD**	**COR**	**STE**
SF	0.0000	0.7156	0.8727	8.9010
VD	0.7156	0.0000	1.3053	8.5980
COR	0.8727	1.3053	0.0000	9.0111
STE	8.9010	8.5980	9.0111	0.0000

Table 34: RMSVD error on the turbulent air sequence

NRMSVD	SF	VD	COR	STE
SF	0.0000	0.0683	0.0833	0.8499
VD	0.0708	0.0000	0.1292	0.8510
COR	0.0830	0.1242	0.0000	0.8573
STE	1.6531	1.5968	1.6736	0.0000

Table 35: NRMSVD error on the turbulent air sequence

ANGULARERROR	SF	VD	COR	STE
SF	0.0000	2.7760	4.1918	60.0272
VD	2.7760	0.0000	5.9403	60.3279
COR	4.1918	5.9403	0.0000	60.7752
STE	60.0272	60.3279	60.7752	0.0000

Table 36: Angular error on the turbulent air sequence

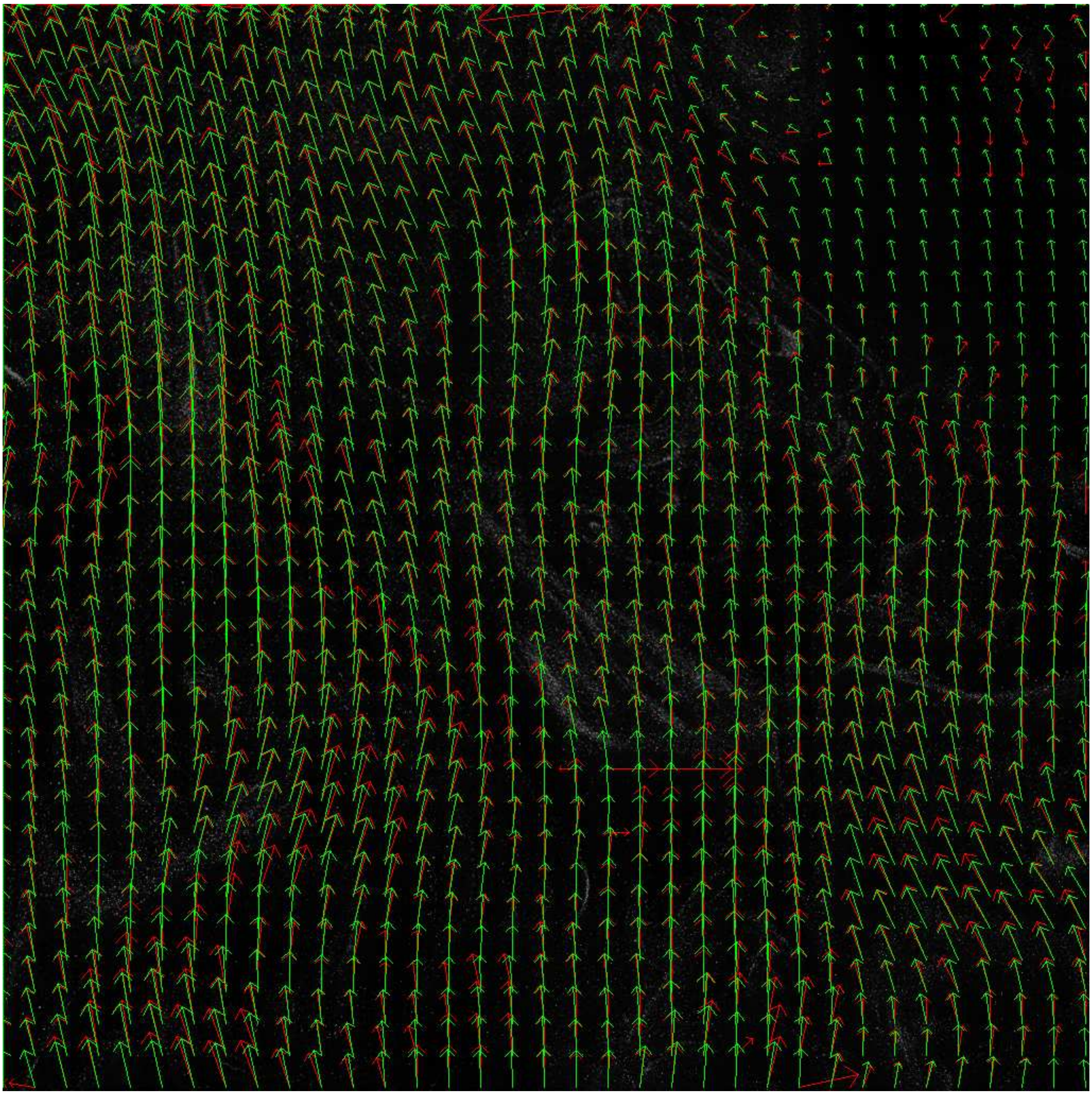

Figure 15: Estimated flow on the real PIV image sequence with turbulent flow (Red: COR, Green: SF)

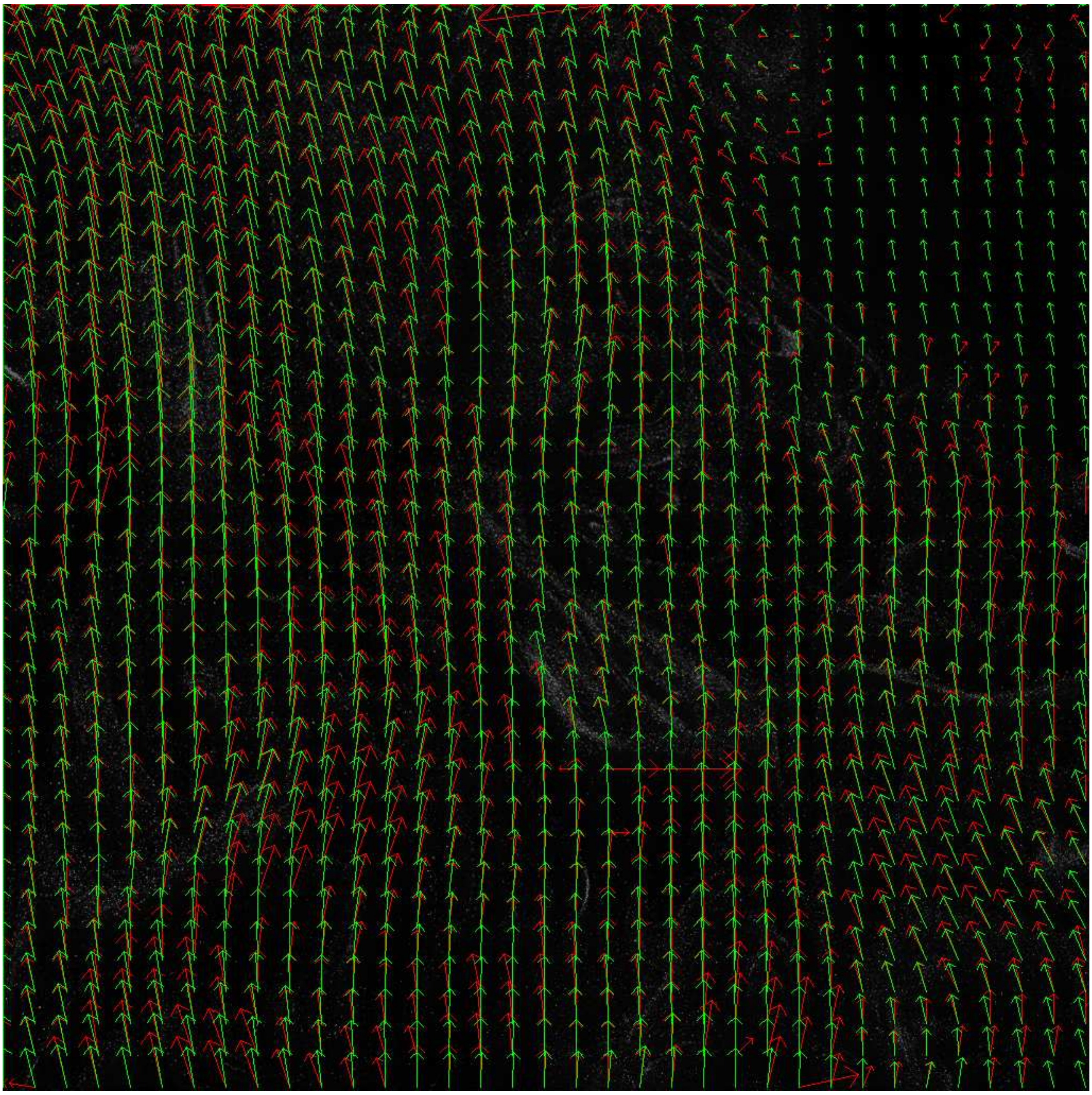

Figure 16: Estimated flow on the real PIV image sequence with turbulent flow (Red: COR, Green: VD)

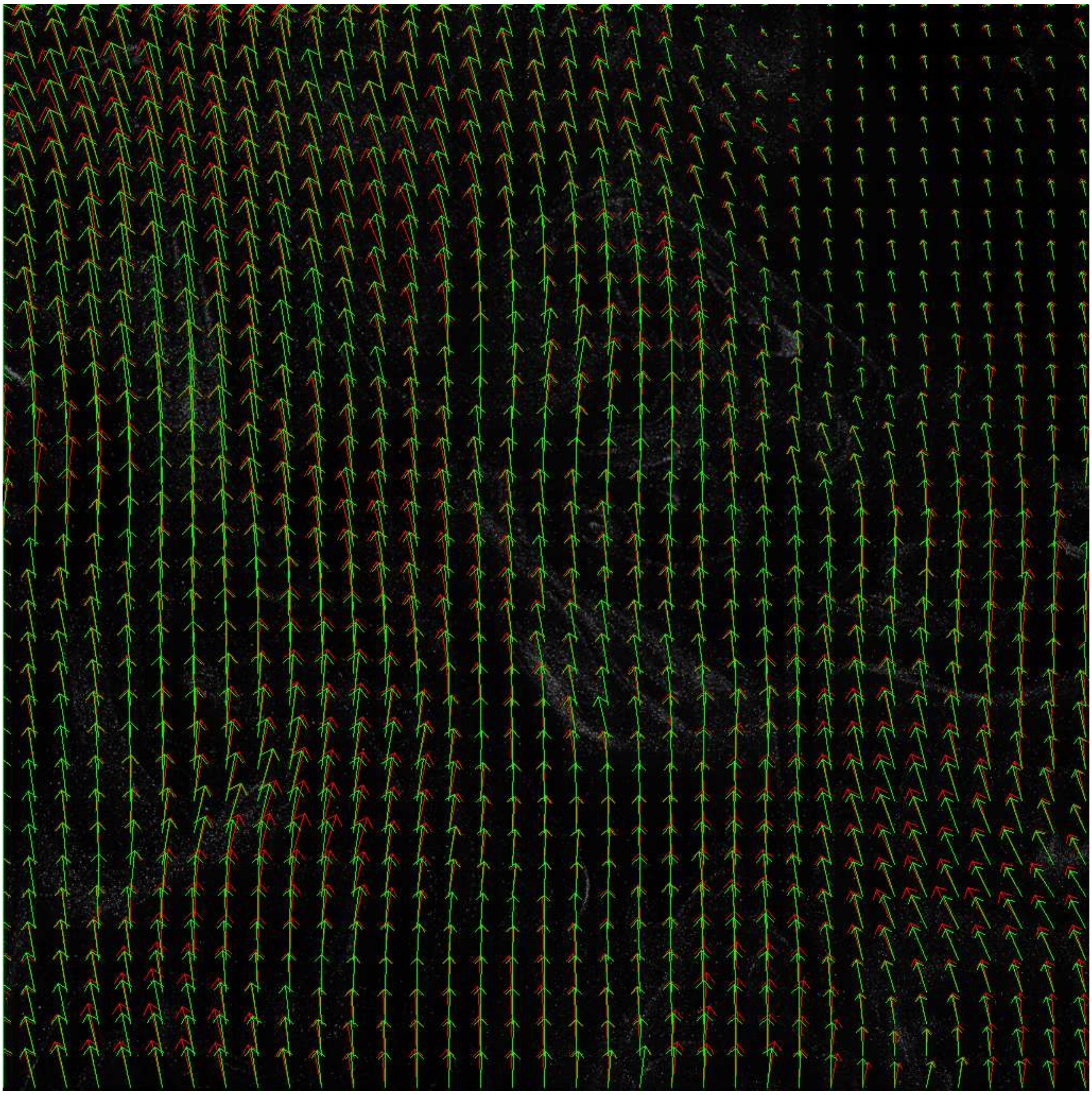

Figure 17: Estimated flow on the real PIV image sequence with turbulent flow (Red: SF, Green: VD)

3.3 Real MSG datasets:

Finally, to complete our experiments, we are going to study the cloud motion from satellite images provided by the MSG (Meteosat Second Generation) satellite. We will focus on that of the North Atlantic and Guinea Golf on Africa.

3.3.1 North Atlantic Sequence:

Tables from 37 to 40 show a statistical analysis of the results obtained for North Atlantic sequence. As it was done before, we compare all the estimation among them to quantify how similar they are since the groundtruth images is unknown. In this sense, we compare the Simple Flow (SF) scheme, the Video Flow (VD) PDE-based estimator, our simple implementation of the correlation based approach (COR) and the structure tensor based approach (STE). As it was expected, simple flow, video flow and correlation approaches provide similar estimated flows since the error among them is lower than one pixel. However, the structure tensor based scheme seems less accurate than the others.

Figure 18 shows the estimated motion vector fields (represented in red (SF), green (VD), dark blue (COR) and light blue (STE)). Figures 19 to 21 show three selected areas of that image in order to visualize the details. As it can be seen, the simple flow based approach provides a continuous and smooth vector field detecting some small motion in areas where there is no motion.

BIAS	SF	VD	COR	STE
SF	0.0000	-0.0864	-0.4283	0.8343
VD	0.0864	0.0000	-0.3415	0.9206
COR	0.4283	0.3415	0.0000	1.2653
STE	-0.8343	-0.9206	-1.2653	0.0000

Table 37: Bias error in the North Atlantic Sequence

RMSVD	SF	VD	COR	STE
SF	0.0000	0.3351	0.6551	1.6004
VD	0.3351	0.0000	0.6035	1.6697
COR	0.6551	0.6035	0.0000	1.7557
STE	1.6004	1.6697	1.7557	0.0000

Table 38: RMSVD error in the North Atlantic Sequence

NRMSVD	SF	VD	COR	STE
SF	0.0000	0.2779	0.5433	1.3273
VD	0.2994	0.0000	0.5392	1.4919
COR	0.8446	0.7780	0.0000	2.2635
STE	0.7842	0.8182	0.8603	0.0000

Table 39: NRMSVD error in the North Atlantic Sequence

ANG. ERR.	SF	VD	COR	STE
SF	0.0000	10.2338	21.8998	36.3755
VD	10.2338	0.0000	20.9141	37.6123
COR	21.8998	20.9141	0.0000	52.6080
STE	36.3755	37.6123	52.6080	0.0000

Table 40: Angular Error in the North Atlantic Sequence

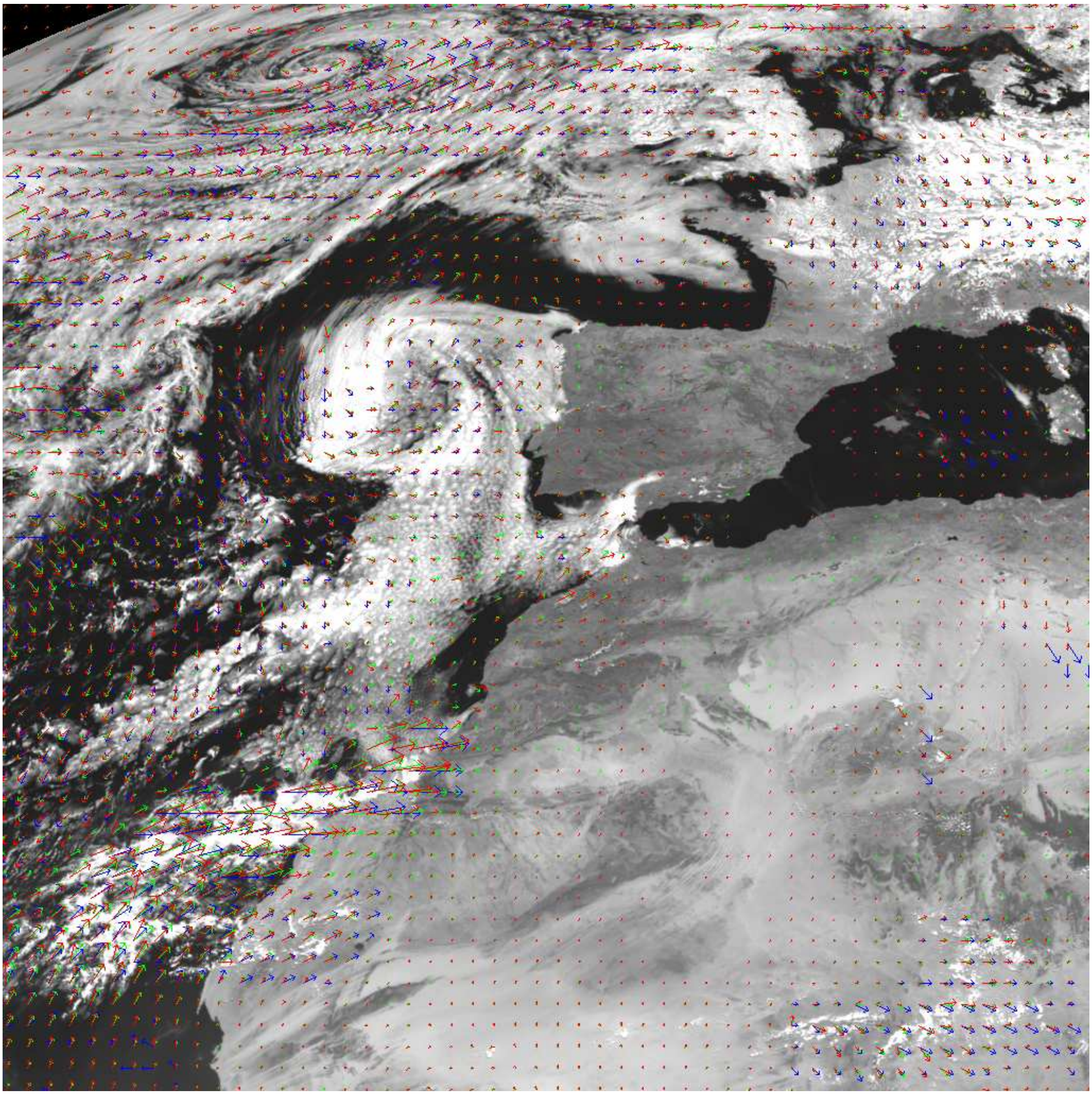

Figure 18: Estimated flow on the North Atlantic image sequence (Red: SF, Green: VD, Dark Blue: COR, Light Blue: STE)

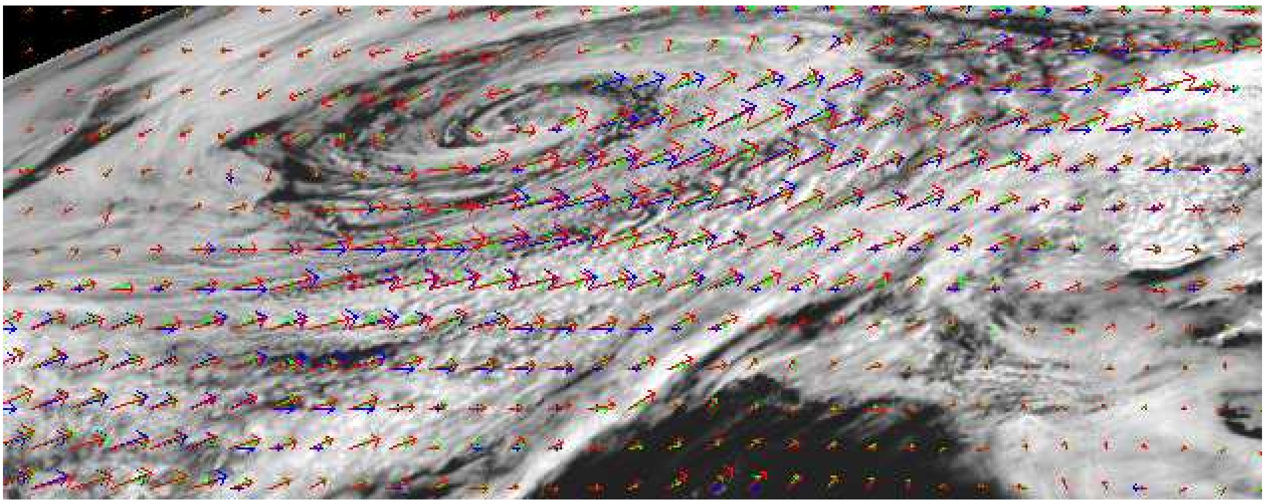

Figure 19: Selection of the estimated flow on the North Atlantic image sequence (Red: SF, Green: VD, Dark Blue: COR, Light Blue: STE)

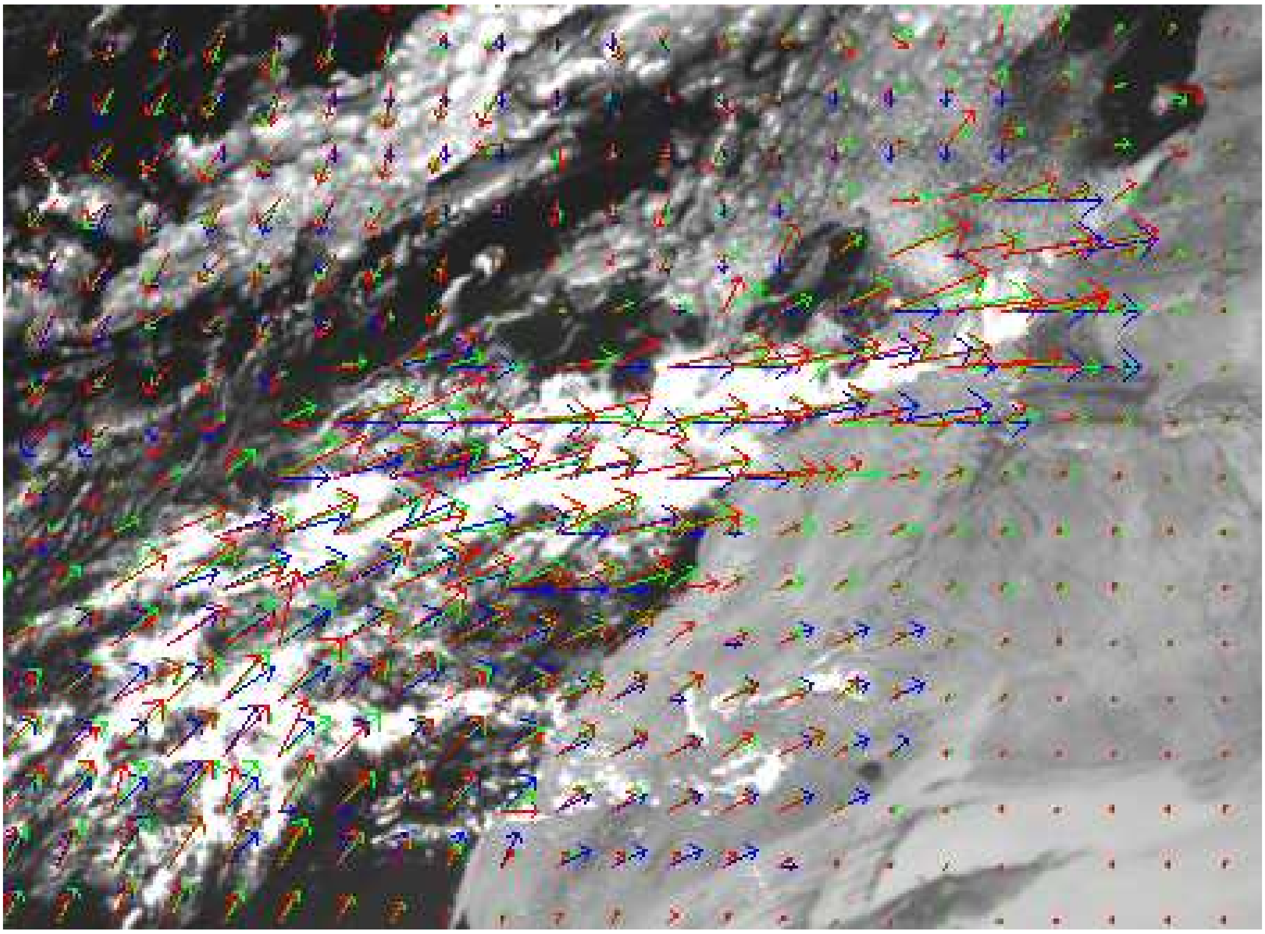

Figure 20: Selection of the estimated flow on the North Atlantic image sequence (Red: SF, Green: VD, Dark Blue: COR, Light Blue: STE)

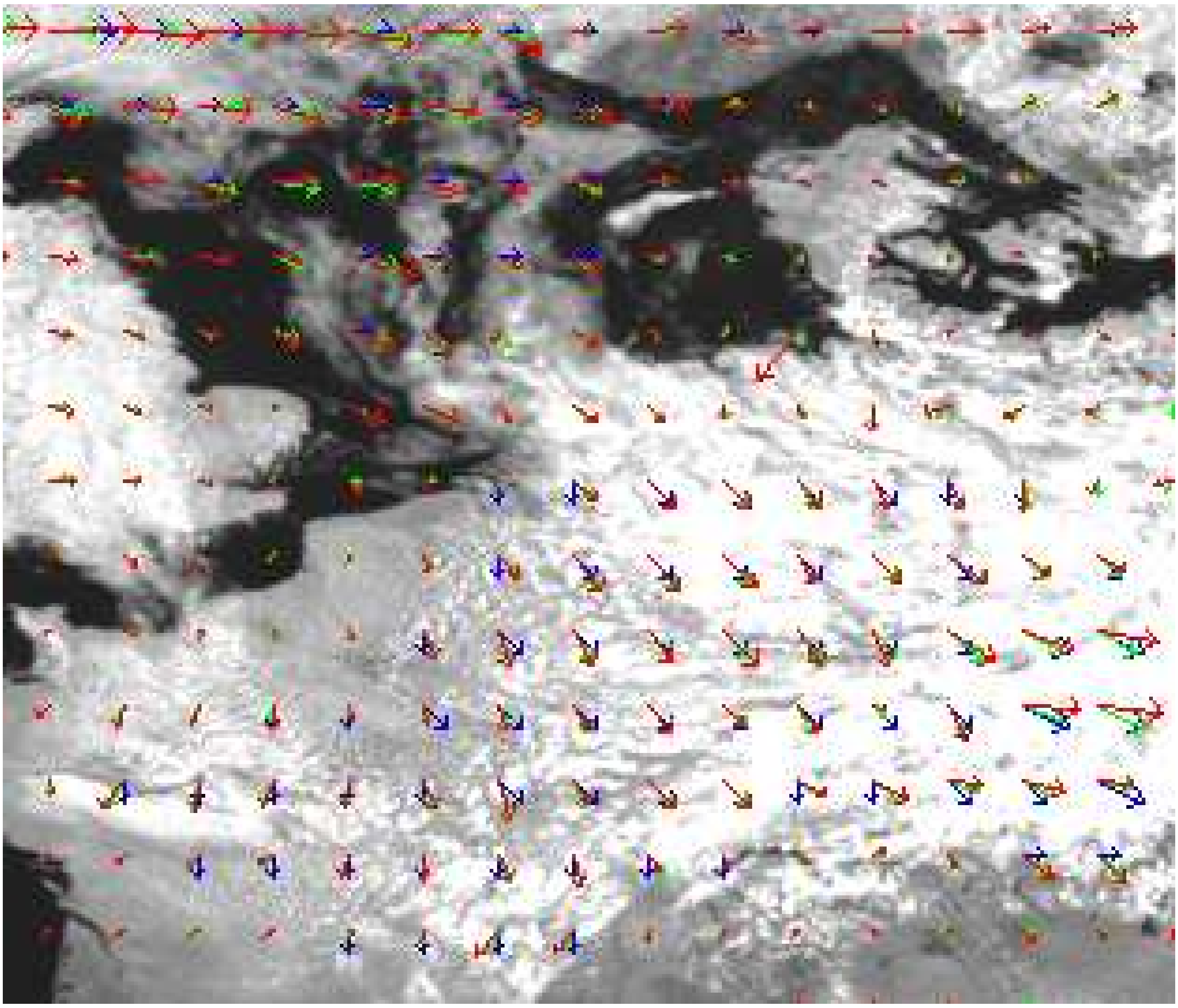

Figure 21: Selection of the estimated flow on the North Atlantic image sequence (Red: SF, Green: VD, Dark Blue: COR, Light Blue: STE)

3.3.2 African Sequence:

Finally, Tables from 41 to 44 show a statistical analysis of the results obtained for North Atlantic sequence. In this case we follow the same procedure for the North Atlantic sequence and the same remarks can be done for this sequence. Figure 22 shows the estimated motion vector fields (represented in red (SF), green (VD), dark blue (COR) and light blue (STE)) and Figures from 23 to 25 show three details of the global image.

BIAS	SF	VD	COR	STE
SF	0.0000	-0.3606	-0.2313	1.3853
VD	0.3606	0.0000	0.1292	1.7461
COR	0.2313	-0.1292	0.0000	1.6175
STE	-1.3853	-1.7461	-1.6175	0.0000

Table 41: Bias in the African Sequence

RMSVD	SF	VD	COR	STE
SF	0.0000	0.6486	0.8286	2.5138
VD	0.6486	0.0000	0.9224	2.6094
COR	0.8286	0.9224	0.0000	2.6677
STE	2.5138	2.6094	2.6677	0.0000

Table 42: RMSVD error in the African Sequence

NRMSVD	SF	VD	COR	STE
SF	0.0000	0.4122	0.5267	1.5978
VD	0.5349	0.0000	0.7607	2.1520
COR	0.6174	0.6873	0.0000	1.9877
STE	0.8490	0.8813	0.9010	0.0000

Table 43: NRMSVD error in the African Sequence

ANG. ERR.	SF	VD	COR	STE
SF	0.0000	17.0547	22.1988	46.0725
VD	17.0547	0.0000	24.7827	48.5289
COR	22.1988	24.7827	0.0000	55.6954
STE	46.0725	48.5289	55.6954	0.0000

Table 44: Angular Error in the African Sequence

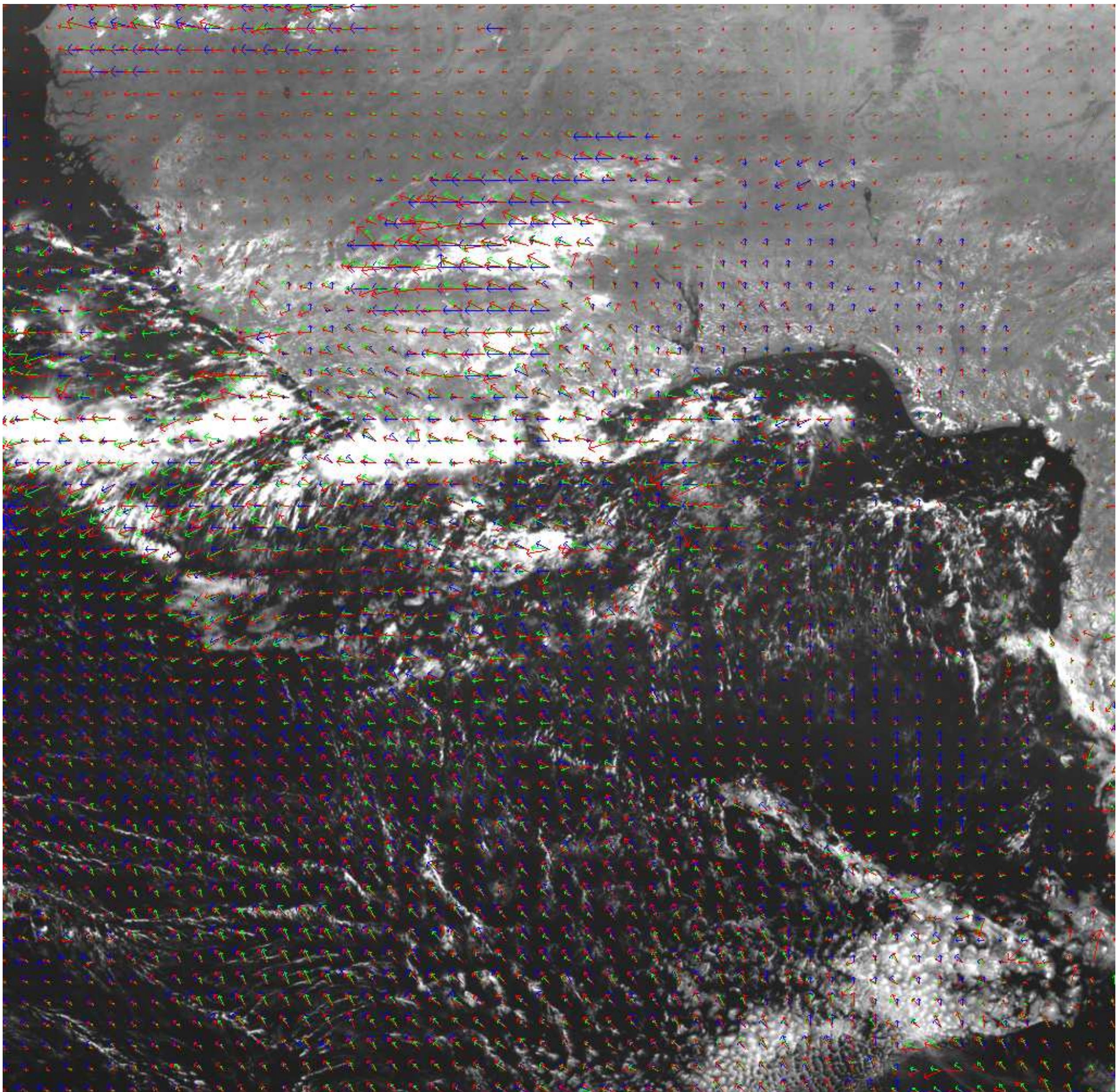

Figure 22: Estimated flow on the African image sequence (Red: SF, Green: VD, Dark Blue: COR, Light Blue: STE)

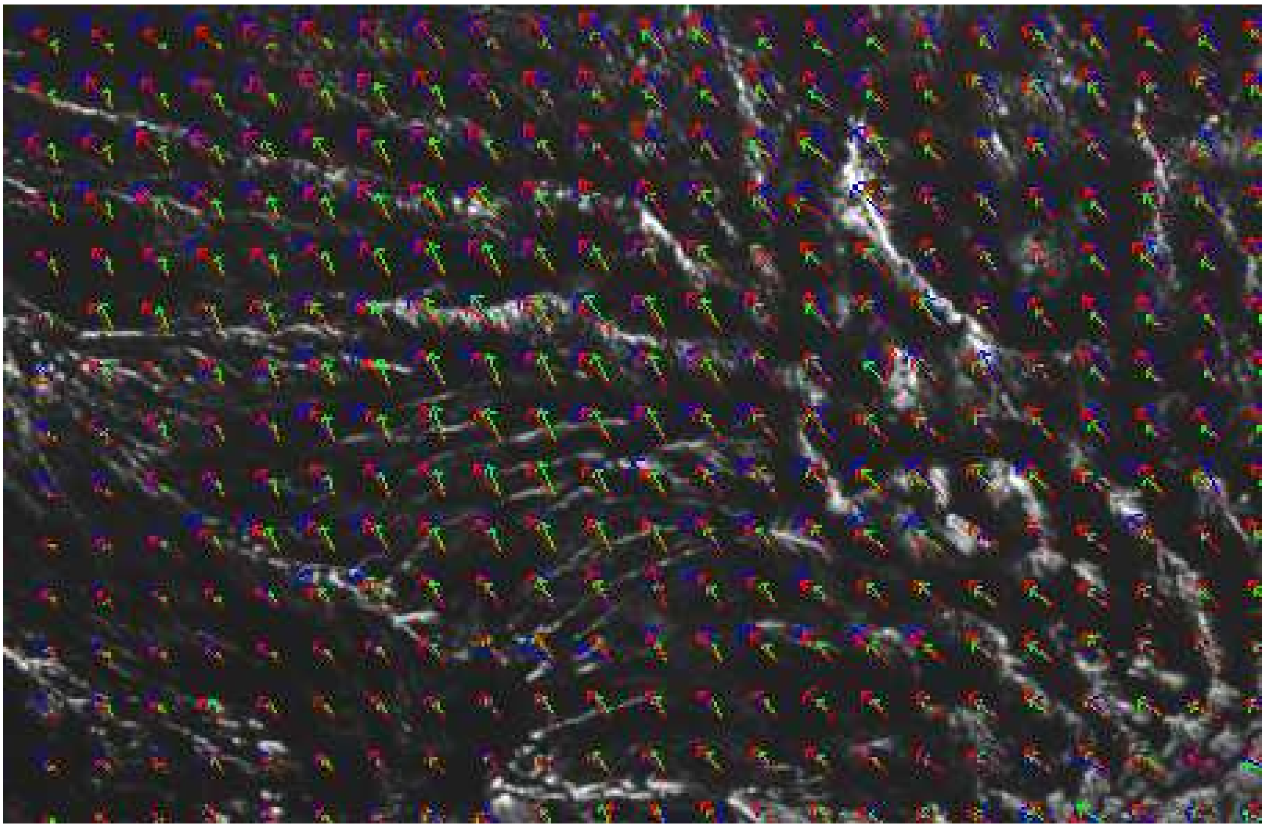

Figure 23: Selection of the estimated flow on the African sequence (Red: SF, Green: VD, Dark Blue: COR, Light Blue: STE)

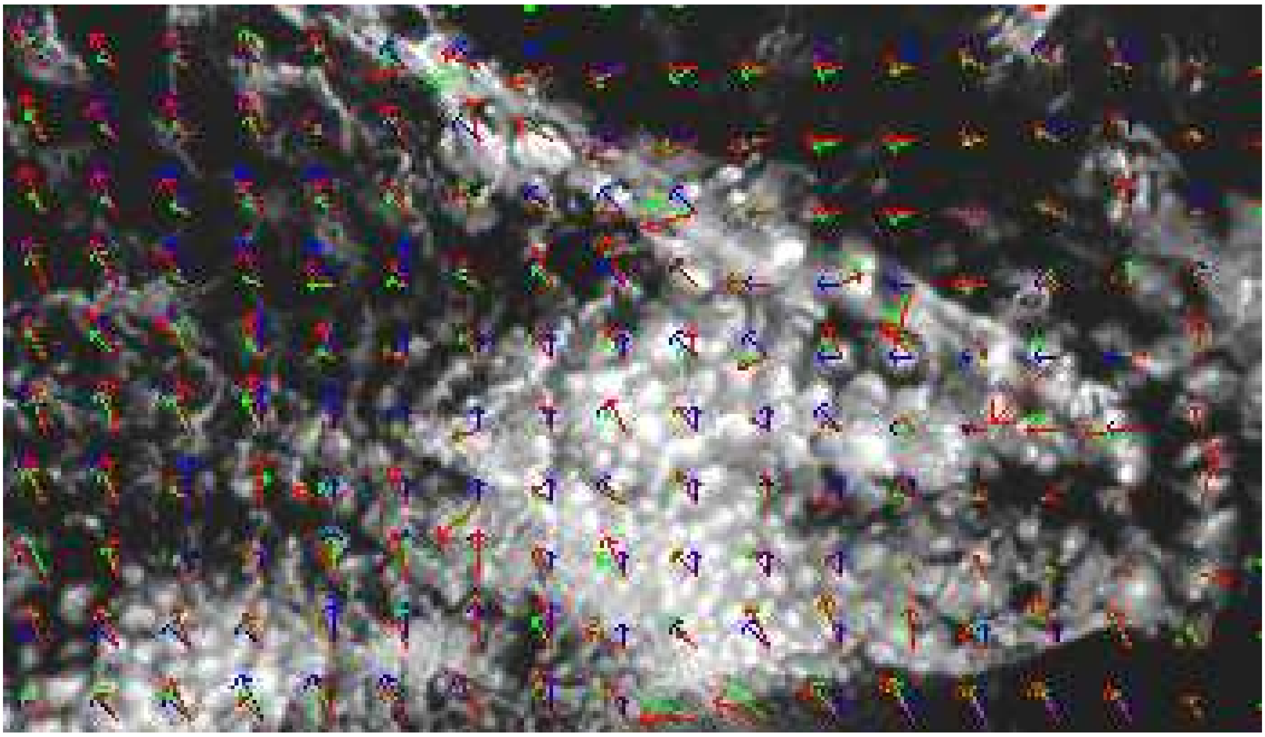

Figure 24: Selection of the estimated flow on the African sequence (Red: SF, Green: VD, Dark Blue: COR, Light Blue: STE)

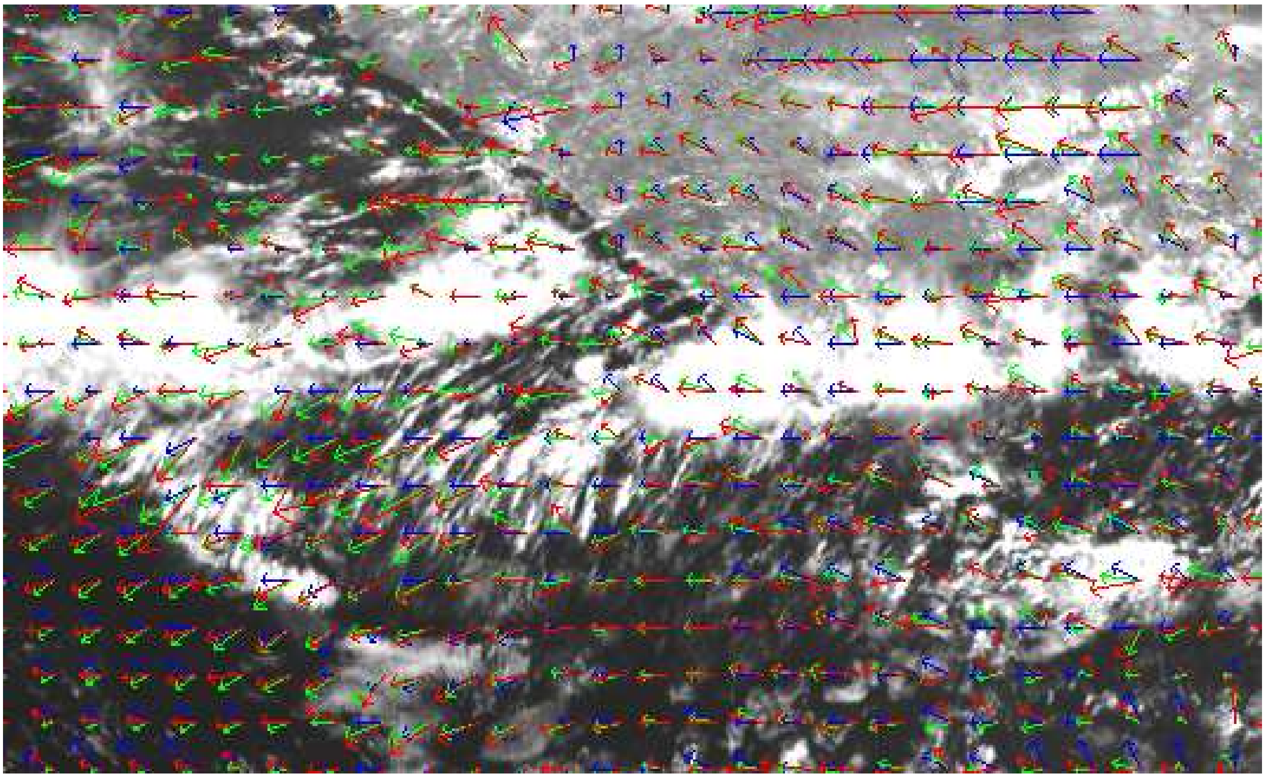

Figure 25: Selection of the estimated flow on the North Atlantic image sequence (Red: SF, Green: VD, Dark Blue: COR, Light Blue: STE)

4 Conclusions

In this report, we propose a common framework to evaluate different optic flow estimation methods in the context of the FLUID Specific Targeted Research Project - Contract No 513633 founded by the EEC. The main goal of this report is, on the one hand, to try to unify the methodological issues in order to be able to share information and conclusions between the partners involved on this project. On the other hand, we analyse the behaviour of four different optic flow estimators in the context of some fluid image sequences in order to identify the main advantage and limitations of the different methods concerning fluid flow sequences.

Since this evaluation procedure is based on a standard ASCII file format, the results provided by any partner can be easily interchanged and compared to any method, independently of the optic flow method implementation, which is seen as a black box. Furthermore, in synthetic experiments we obtain both quantitative and qualitative information about the performance of the methods we would like to characterize.

Nevertheless, when working with real image sequences it is very difficult to obtain the groundtruth motion vector field in order to get an error classification. Hence, we are obliged to take conclusions from synthetic sequences which is interesting, but could be misleading. In this sense, the FLUID partners have provided an interesting dataset of PIV synthetic image sequences, but it would be desirable to perform a similar analysis with synthetic satellite images, which have not been provided, to complete the comparison work.

Concerning the evaluation of the four methods compared in this report, we can conclude that for very simple flows all the methods provide a good performance since the error is always quite low. However, as the flow becomes more complex (that is, also includes orientation variation) and more realistic, the results provided by the structure tensor approach is quite inaccurate while the error provided by PDE based schemes (Simple Flow and Video Flow) and the correlation based approach are quite similar, although a further study can be done to improve the results provided by these methods.

References

[1] First set of fluid mechanics image sequences, Draft, AEROBIO-CEMAGREF (March 2005).

[2] F. Scarano, B. Wieneke, Compact test image on spatial resolution, Draft, World Wide Cooperation on Particle Image Velocimetry - PIV Challenge (Sept. 2005).

[3] B. Wieneke, Description of 3d-synthetic data, Draft, LaVision (November 2005).

[4] A. Szantai, F. Désalmand, Report 1: Basic information on msg images, Draft, Laboratoire de Météorologie Dynamique (August 2005).

[5] M. Alemán, L. Alvarez, E. González, L. Mazorra, J. Sánchez, Optic flow estimation in fluid images I, Cuadernos Instituto Universitario de Ciencias y Tecnologías Cibernéticas 31 (2005) 1–25.

[6] A. Salgado, J. Sánchez, Spatio-temporal optical flow estimation with large displacements, in: (Preprint), 2005.

[7] F. Becker, J. Yuan, C. Schnörr, Deliberable 2.2. demonstrator on multiscale motion estimation, Draft, CVGPR. University of Mannheim (November 2005).

[8] J. Yuan, F. Becker, C. Schnörr, Report on filter bank design for local fluid motion estimation, Draft, CVGPR, University of Mannheim (November 2005).

Instituto Universitario de Ciencias y Tecnologías Cibernéticas
Universidad de Las Palmas de Gran Canaria
Campus de Tafira
35017 Las Palmas, España
http://www.iuctc.ulpgc.es